Computational fluid-dynamics investigations of vortex generators for flow-separation control

by

Florian von Stillfried

Doctoral Thesis

Royal Institute of Technology
School of Engineering Sciences
Linné FLOW Centre
Department of Mechanics
SE - 100 44 Stockholm

Akademisk avhandling som med tillstånd av Kungliga Tekniska högskolan i Stockholm framlägges till offentlig granskning för avläggande av teknologie doktorsexamen onsdagen den 16 maj 2012 kl. 10:15 i F3, Lindstedtsvägen 26, Kungliga Tekniska högskolan, Stockholm.

US–AB, Stockholm 2012

Abstract

Many flow cases in fluid dynamics face undesirable flow separation due to adverse pressure gradients on wall boundaries. This occurs, for example, due to geometrical reasons as in a highly curved turbine-inlet duct or on flow-control surfaces such as wing trailing-edge flaps within a certain angle-of-attack range. Here, flow-control devices are often used in order to enhance the flow and delay or even totally eliminate flow separation. Flow control can e.g. be achieved by using passive or active vortex generators (VGs) for momentum mixing in the boundary layer of such flows. This thesis focusses on such passive and active VGs and their modelling for computational fluid dynamics investigations.

First, a statistical VG model approach for passive vane vortex generators (VVGs), developed at the Royal Institute of Technology Stockholm and the Swedish Defence Research Agency, was evaluated and further improved by means of experimental data and three-dimensional fully-resolved computations. This statistical VVG model approach models those statistical vortex stresses that are generated at the VG by the detaching streamwise vortices. This is established by means of the Lamb-Oseen vortex model and the Prandtl lifting-line theory for the determination of the vortex strength. Moreover, this ansatz adds the additional vortex stresses to the turbulence of a Reynolds-stress transport model. Therefore, it removes the need to build fully-resolved three-dimensional geometries of VVGs in a computational fluid dynamics mesh. Usually, the generation of these fully-resolved geometries is rather costly in terms of preprocessing and computations. By applying VVG models, the costs are reduced to that of computations without VVGs. The original and an improved calibrated passive VVG model show sensitivity for parameter variations such as the modelled VVG geometry and the VVG model location on a flat plate in zero- and adverse-pressure-gradient flows, in a diffuser, and on an airfoil with its high-lift system extracted. It could be shown that the passive VG model qualitatively and partly quantitatively describes correct trends and tendencies for these different applications.

In a second step, active vortex-generator jets (VGJs) are considered. They were experimentally investigated in a zero-pressure-gradient flat-plate flow at Technische Universität Braunschweig, Germany, and have been re-evaluated for our purposes and a parameterization of the generated vortices was conducted.

Dependencies of the generated vortices and their characteristics on the VGJ setup parameters could be identified and quantified. These dependencies were used as a basis for the development of a new statistical VGJ model. This model uses the ansatz of the passive VVG model in terms of the vortex model, the additional vortex-stress tensor, and its summation to the Reynolds stress tensor. Yet, it does not use the Prandtl lifting-line theory for the determination of the circulation but an ansatz for the balance of the momentum impact that the VGJ has on the mean flow. This model is currently under development and first results have been evaluated against experimental and fully-resolved computational results of a flat plate without pressure gradient.

Descriptors: flow-separation control, vane vortex generator, vortex generator jet, zero-pressure-gradient turbulent boundary layer, adverse-pressure-gradient turbulent boundary layer, statistical modelling, turbulence, Reynolds stress-transport model, computational fluid dynamics

Preface

This doctoral thesis is written within the area of fluid mechanics and mainly investigates computational studies regarding vortex generators. In particular, this thesis examines statistical vortex-generator models which were applied in wall-bounded turbulent flows. One main focus of this work was a thorough evaluation study of passive vortex-generator models and its application in zero- and adverse-pressure-gradient flat-plate boundary-layer flows, in asymmetric diffuser flow, as well as on an airfoil with a deployed short-chord flap. Another main focus of this contribution was to parameterize and model the vortices from vortex-generator-jet experiments that were carried out at Technische Universität Braunschweig, Germany, and to determine the model parameter dependencies on the experimental vortex-generator-jet setup parameters. As a result, a new formulation for a statistical vortex-generator-jet model was derived and evaluated against experimental and fully-resolved computational results.

This thesis is subdivided into two parts. In the first part, background on vortex generators, the governing equations, the basic concepts and methods for the statistical-modelling approach, and a short discussion of selected results are presented. The second part of this thesis includes in total four journal papers, three of them either published or accepted for publication, and which are adjusted to comply with the present thesis format, as well as one conference proceedings paper. A digital version of this thesis is available for download on the KTH library homepage on *http://www.kth.se/en/kthb*.

Stockholm, May 2012
Florian von Stillfried

Contents

Abstract iii

Preface v

Part I. Overview and summary

Chapter 1. Introduction 1

Chapter 2. Background 4
2.1. Passive Vane Vortex Generators 4
2.2. Active Vortex Generator Jets 7

Chapter 3. Governing Equations 10

Chapter 4. Vortex Generator Modelling 13
4.1. Existing Vane Vortex Generator Models 13
4.2. User Challenges of VG Models 15
4.3. Statistical Vortex Generator Models 16
4.4. Statistical Vane Vortex Generator Model 19
4.5. Statistical Vortex Generator Jet Model 24

Chapter 5. Selected Results and Discussion 28
5.1. Original VVG Model in APG Flat-Plate Flow 28
5.2. Comparison of the VVG models 28
5.3. VVG Model Applications 32
5.4. Parameterization of VGJ Experiments 34
5.5. Evaluation of the Statistical VGJ Model 36

Chapter 6. Summary of Appended Papers 39

Chapter 7. Concluding Remarks and Outlook 43

Chapter 8. Papers and Authors' Contributions 45

Acknowledgements 48

References 50

Part II. Papers

Paper 1. Vortex-Generator Models for Zero- and Adverse-Pressure-Gradient Flows 57

Paper 2. Evaluation of a Vortex Generator Model in Adverse Pressure Gradient Boundary Layers 89

Paper 3. Evaluating and Parameterizing Round Vortex-Generator Jet Experiments for Flow Control 121

Paper 4. A Statistical Vortex-Generator-Jet Model for Turbulent Flow-Separation Control 157

Paper 5. Application of a Statistical Vortex Generator Model on the Short-Chord Flap of a Three-Element Airfoil 183

Part I

Overview and summary

CHAPTER 1

Introduction

The demand to design more efficient flow-separation control systems such, for example, new high-lift configurations for future aircraft which enable better low-speed behaviour during takeoff and landing, increased safety, and less environmental impact is becoming more important for the aircraft industry. At the same time, reduction of the complexity of existing flow-separation control systems is not only a trend but necessary in order to, for the example of a high-lift system, advance flight safety, reduce overall weight, lower fuel emissions, increase the operating distance, just to mention a few. For this case, it can be stated that the high-lift system has a meaningful impact on the total performance of the aircraft, economically as well as ecologically. Not only the aircraft industry faces such demands, other industries that develop and use fluid-mechanical processes are constantly in the need to improve products to either be and remain competitive, and/or to fulfil legal requirements as, for example, certification processes due to changing regulations on different markets throughout the world.

Flow-separation control can be a very effective way for improving existing fluid-dynamical systems, and a powerful tool in the conceptual design process from the very beginning of a product-development cycle. The term "flow-separation control" in fluid dynamics is generally used when a wall-bounded fluid flow is modified by flow-separation-control devices such as, for example, vortex generators (VGs). The general benefit from applying VGs in wall-bounded flows is a possible delay and/or prevention of boundary-layer separation and thereby, an increase of the overall system efficiency. In the limit of the operational envelope, fluid-dynamical systems may not perform properly without flow-separation control.

When flow-separation control is necessary, equipping control surfaces with VGs is a common procedure; see figures 1.1 and 1.2. Such VGs mix the fluid near those surfaces and push higher-momentum-containing fluid closer towards the wall, and vice versa. This increases the near-wall velocity and the near-wall momentum, and consequently the stability of the flow in terms of separation delay and/or prevention. During a product-development phase, an increasing amount of computational analysis is used nowadays, and VGs generally have the disadvantage of being computationally costly and time-consuming when included in a detailed analysis. Computational grids often fully resolve VGs, leading to a large amount of additional nodes in their vicinity, which causes

FIGURE 1.1. Deployed flaps and spoilers uncover VGs close to the leading edge on a flap during landing.

FIGURE 1.2. VGs against buffeting effects on a main wing during cruise flight.

high computational costs. Therefore, VGs are often neglected in computational analyses. In a later stage during an experimental evaluation, VGs are, on the other hand, often included in for example wind- or water-tunnel investigations so that their impact can be studied thoroughly. This is a disadvantage for the product-design process that may benefit from a detailed computational analysis from the very beginning of the product-development cycle.

Different techniques to include VGs in computations are typically used: fully-resolved, partly-resolved, and fully-modelled approaches exist. Fully-resolved three-dimensional VGs and corresponding vortex structures are fully

embedded in the computational mesh, typically leading to very fine mesh sizes in their vicinity. Partly-resolved approaches model the VGs by, for example, volume forces that are added to the governing equations. Still, the generated vortex structures need to be fully resolved and a high mesh density, comparable to the fully-resolved approach, is needed downstream of the VGs. Fully-modelled approaches go one step further: they also model the generated vortex structures downstream of the modelled VGs. This approach further reduces the mesh size compared to the partly-resolved approach. Nevertheless and due to the increased modelling, it is necessary to further verify results for the partly- and the fully-modelled approaches by means of comparisons against experimental and/or fully-resolved computational results.

This thesis mainly discusses the development and evaluation of fully-modelled VG models for passive and active flow-separation control and provides comparative studies regarding fully-resolved computational analyses and experiments. It includes the application and the evaluation of a statistical method that may be used for including VGs in a computational analysis during the early design process. A considerable advantage of the statistical method is that it removes the actual need to include VG geometries and vortex structures within a computational grid. Normally, this leads to a significant larger number of nodes and thus, longer preprocessing, computation and postprocessing time. Instead, the physical impact of the vortices on the mean flow in terms of additional vortex stresses is modelled. This results in negligible additional computational costs when compared to computations without flow-separation control, but to tremendous savings when compared to three-dimensional computations with fully-resolved VGs.

CHAPTER 2

Background

Vortex generators generate streamwise vortex structures that typically mix the boundary layer in wall-bounded flows. This increases the mean-streamwise velocity near the wall, as well as an average momentum transport towards it. As a result, the boundary-layer velocity profile becomes fuller where high-momentum fluid is pushed towards the wall and less full where it is pushed away. In total, VGs maintain the flow to be more stable by boundary-layer mixing processes, resulting in delayed or even prevented boundary-layer separation. In the following, previous findings from research regarding passive and active VGs are presented.

2.1. Passive Vane Vortex Generators

For quite some time, passive vane vortex generators (VVGs) have been used in order to control flow separation. "Passive" refers to VGs that generate a streamwise vortex without requiring additonal external energy. However, the additional benefit of using passive VVGs generally comes along with a somewhat increased overall drag. A way to avoid this drag penalty is to use VVGs that can be retracted when not needed, as can be seen for the adjustable control surfaces in figure 1.1. The presence of parasitic drag is a tradeoff situation for the designer, whereas it is not easy to predict drag penalties and the disadvantages of a fixed passive VVG system a priori. Typically, VVGs are installed normal to the surface, with a vane angle of incidence α towards the mean-flow direction. Flow-separation control with passive VVGs is by far the cheapest and fastest way to equip solid bodies and is therefore widely used in aeronautics and related industries nowadays. Many different research groups have evaluated VVGs experimentally and by means of computations, and it is well-proven that these devices can efficiently increase the overall performance of fluid-mechanical systems.

Pearcey (1961) suggested certain design criteria for successful boundary-layer flow control with VVGs. His studies encompassed different VVG designs as for example corotating and counter-rotating VGs, multiple-row systems, and VVGs of different geometries; see also figure 2.1. "Counter-rotating" setups, see figure 2.2(a), typically contain VVG pairs with vanes mounted in a mirror-inverted manner so that vortices with opposite-rotational directions are generated. This arrangement is common for the application of flow-separation control in two-dimensional flows when the spanwise velocity component is zero,

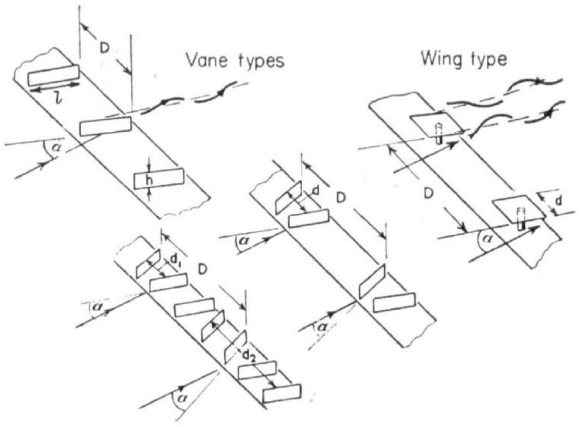

FIGURE 2.1. Types and notation of Pearcey's VVGs. [From Pearcey (1961).]

also used in this thesis. In contrast to that are "co-rotating" setups, see figure 2.2(b), where VVG vanes are installed in the same manner regarding α and therefore, produce vortices with the same rotational directions. This arrangement is typically found in three-dimensional flows on, for example, highly swept aircraft wings with strong cross-flows. Pearcey investigated parameters like the distance D between neighbouring VVG pairs, the distance d between two VVG vanes of a VVG pair, the VVG chord c[1], and the vane angle of incidence α. By that, Pearcey carried out one of the most important studies for passive VVGs already more than 50 years ago.

More recent studies (Lin 2002; Yao *et al.* 2002) have shown that so-called subboundary-layer VVGs (SBVGs) have major advantages compared to standard VVGs with vane heights in the order of the local boundary-layer thickness δ_{99}, i.e., $h_{\mathrm{VG}}/\delta_{99} \approx 1$. SBVGs have a typical device height of $0.1 \leq h_{\mathrm{VG}}/\delta_{99} \leq 0.5$, thus mixing the mean-flow momentum only within the boundary layer. This has been shown to be very efficient compared to standard VVGs. The VVGs which were studied in this thesis can be considered as SBVGs (although, $h_{\mathrm{VG}}/\delta_{99} \approx 0.65$ for the defined baseline VVG position in von Stillfried *et al.* (2011*b*,*a*)). A VVG streamwise-position variation study increased the ratio $h_{\mathrm{VG}}/\delta_{99}$ upstream of the baseline VVG position, and a decrease in skin-friction results could be observed, basically confirming Lin's findings.

A comprehensive research study for passive VVGs with counter- and corotating setups was carried out by Godard & Stanislas (2006) which was partly based on the findings from Lin (2002). Their motivation was to describe optimal parameters for VVGs for the flow over a bump, similar to the suction

[1]In this thesis, c is defined as the streamwise projected VVG chord, i.e., the length of the chord along the VVGs becomes $c/\cos\alpha$.

side of an airfoil. For that, they studied previous results by several research groups and started from the optimal parameters given in Lin *et al.* (1991). By successively varying the VVG parameters and measuring the overall performance in terms of skin-friction distributions at two spanwise symmetry planes, they could define optimum settings both for the counter- and the corotating systems. In terms of h_{VG}, Godard & Stanislas identified that the skin-friction distributions increased with increasing h_{VG}, which is in contrast to some results in existing literature. As a result of the study, Godard and Stanislas found that "the counter-rotating configuration is twice as efficient as the corotating one, which is already quite efficient". The setup for the optimum counter-rotating case by Godard & Stanislas is very close to the setup used by Lögdberg *et al.* (2009) in the two-dimensional flat-plate boundary-layer experiments that were also utilized in the present work.

Pauley & Eaton (1988) have experimentally investigated VVG pairs and arrays with a ratio $h_{\mathrm{VG}}/\delta_{99} = 1.5$, mounted in a zero-pressure-gradient (ZPG) flat-plate boundary layer, and mainly investigated spanwise vorticity contours. Different VVG setups were examined, as for example counter-rotating common-flow-up/down, pairs with different height ratios $h_{\mathrm{VG}}/\delta_{99}$, corotating and alternating arrays. They varied the angle of incidence α as well as the spacing d, and could show that a strong interaction of neighbouring vortices (for example, common-flow-up settings) caused a decrease of peak vorticity, whereas the streamwise development of the vortex circulation was primarily connected to the interaction with the wall and thus, skin friction. Vortices that were located closer to the wall (for example, counter-rotating common-flow-down setups) caused a larger skin-friction variation which, in turn, diminished the circulation. A conclusion of their work is that VVG pairs should be arranged in such a way that they produce common-flow-down vortex structures which could be confirmed by the results given in this thesis. Furthermore, corotating VVG

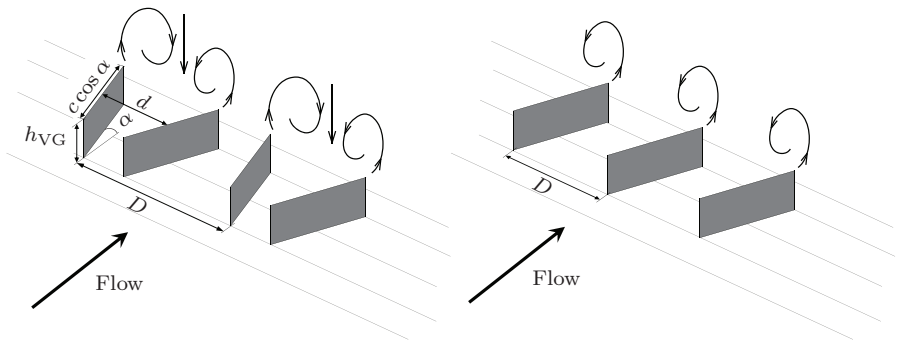

(a) (b)

FIGURE 2.2. VVG setups and the notation that is used in this thesis: (a) counter-rotating common-flow-down, and (b) corotating ($d = 0$) configurations.

arrays should provide a certain minimum distance D because vortex velocities may cancel out each other if VVGs are located too closely to each other.

Another interesting work was published by Barth *et al.* (2011), who have examined a dynamical VVG system which deploys/retracts the VVG actuators at very high frequencies. Their motivation was to investigate high-frequency and dynamically-retractable VVGs due to the general setup limitations for high-frequency blowing by active vortex-generator jets. Barth *et al.* (2011) could for example show that the dynamic VVGs mix the boundary layer by large-scale momentum and not as an effect of the turbulence scales, which supports the findings of Ortmanns & Kähler (2007) for vortex-generator jets; see also section 2.2. These results form an important information for the statistical modelling approaches which utilize the findings of Ortmanns & Kähler (2007) and Barth *et al.* (2011). Basically, it was shown that flow-separation is established by the large-scale momentum mixing from the streamwise vortices, and this concept is used for the statistical VG models which are presented in this thesis.

2.2. Active Vortex Generator Jets

Even though the concept of active flow control was investigated already as early as in the middle of the 20^{th} century, it has only become more popular in the research community during the last 25 years. Unlike passive VVGs, active VGJs usually do not include any geometrical structures which penetrate from the surface into the mean flow. This has the advantage that VGJs do not contribute to parasitic drag in contrast to permanently deployed VVGs. Moreover, VGJs have the option to be activated when flow-separation control is needed, and to be deactivated when flow control is not needed. This feature makes this concept highly flexible and efficient.

VGJs create vortices by means of an injected jet with a velocity U_{VGJ} which enters the boundary-layer flow through the actuator exit of diameter Φ_{VGJ} in a direction characterized by the pitch and skew angles α and β, respectively; see figure 2.3. It is observed that, in this work, the skew angle $\beta = 0°$ is defined in the upstream direction. The jet injection is enabled by means of continuous or pulsating jet blowing. The higher amount of possible setup-parameter combinations make active VGJs, compared to passive VVGs, more complicated and time-consuming to investigate. This is one of the practical reasons for the dominance of experimental investigations in contrast to a smaller amount of computational studies.

Selby *et al.* (1992) present an important parametric study for co- and counter-rotating VGJ arrays, and a variation of the VGJ parameters $\alpha = 15°$ to $90°$, $\beta = 90°$ to $180°$, $\Phi_{\text{VGJ}} = 0.8$ to 4.8 mm, and the velocity ratio $\lambda = U_{\text{VGJ}}/U_\infty = 0.6$ to 6.8. The study has shown by means of pressure-distribution plots that increasing λ generally increased the performance of the flow-control system, which can be confirmed by the findings of an increase in vortex stresses for growing λ in this thesis; see appended Paper 4. In the same

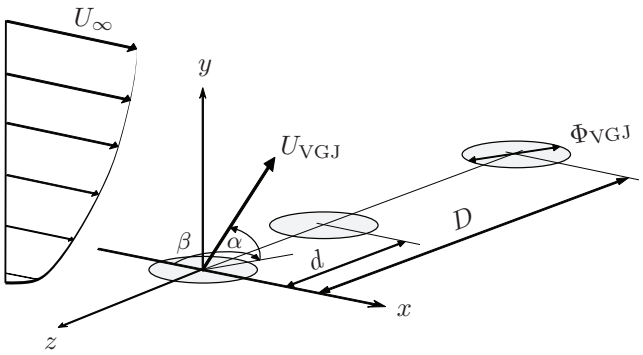

FIGURE 2.3. The VGJ actuator geometry and parameters, also showing the additional symmetry parameters d and D for pair and array configurations.

manner, Selby *et al.* (1992) demonstrated that efficiency increased with increasing α up to 25°, as well as for decreasing β to values between 90° and 120°. Moreover, counter-rotating VGJ arrays showed to have inferior performance when compared to corotating systems.

Also Johnston & Nishi (1990) have studied configurations of skewed and pitched co- and counter-rotating round VGJ arrays. It could be shown for $\beta = 90°$, that the generated streamwise vortices were similar to those from passive VVGs, that the mixing in the boundary layer was associated with the streamwise vortices, and that the vortices successfully eliminated regions of separation. These findings support the similar vortex modelling ansatzes for the VVG and the VGJ models in this thesis. Johnston & Nishi (1990) showed that vortices from VGJs tended to dissipate faster than those from passive VVGs. Compton & Johnston (1992) showed that β between 90° and 135° maximized the vorticity of the streamwise vortex, and that the vortices were comparable to weak vortices from VVGs for velocity ratios $\lambda = 0.7$ to 1.3. In this thesis, it can be found that $\lambda = 2.5$ produces approximately equal strong VGJ vortex stresses when compared to the basic VVG setup by Lögdberg *et al.* (2009). On the other hand, increasing λ to 5.0 amplifies the vortex stresses by one order of magnitude, possibly providing advances for VGJ flow-separation control. Khan & Johnston (2000) investigated a smooth contoured actuator-exit nozzle and identified the strongest peak mean vorticity for $\lambda = 1.0$, $\alpha = 30°$, and $\beta = 120°$. They report a streamwise momentum defect in the vortex core and an increased turbulence level between the vortex and the wall. In another contribution, Johnston *et al.* (2002) investigated the effects of two different round actuator-inlet characteristics (the smooth-contoured actuator nozzle from Khan & Johnston (2000) and a sharp-edged inlet) on the vortex creation under identical boundary conditions. They showed the near-field charateristics for $x/\Phi_{\mathrm{VGJ}} \leq 5$ of the sharp-edged inlet to be very different from the smooth-contoured inlet. This was probably due to the stalled region

which led to area blocking as well as to instabilities of the shear-layer inside the nozzle. A faster dissipation of the dominant vortex is the result, but the influence of the sharp edge damps out for $x/\Phi_{\mathrm{VGJ}} > 10$, with results of both inlets becoming comparable to each other. The experimental results in this thesis provided two different inlet geometries for the single-jet (no duct) and the VGJ pair setup (sharp-edge duct). The findings of Johnston *et al.* (2002) are important for a valuation of results for different actuator inlet geometries, and for a sensitizing concerning the results interpretation.

Zhang & Collins (1997) investigated the near field behind a single round VGJ by means of mean-velocity contours and proposed $\alpha = 30°$ and $\beta = 120°$ for $\lambda = 1.0$ as suitable jet parameters, essentially in agreement with Khan & Johnston (2000). Zhang & Collins (1997) state that a single vortex was developed within $x/\Phi_{\mathrm{VGJ}} \leq 10$, and that the vortex core moved away from the wall with increasing λ. Their findings are generally valid for the VGJ stress results from experiments; see appended Papers 3 and 4. Another important result was that they observed a significant influence of the freestream flow on the jet. Zhang (2003) investigated corotating VGJ arrays at $\alpha = 45°$ and $\beta = 135°$ with the same actuator type and the same boundary conditions as in Zhang & Collins (1997). Zhang claims that the vortices from the VGJ array had the same main characteristics compared to a single VGJ with a similar setup, and a similar presumption was made for the spanwise-averaged second-order statistics of single VGJ from experiments; cf. appended Paper 3. Moreover, Zhang states that, as a consequence of the vortex presence in the flow, turbulence production appeared to be the main mechanism to form the primary shear stresses.

Ortmanns & Kähler (2007) have examined single round VGJs in a water-tunnel flat-plate turbulent boundary layer and have shown that the turbulent fluctuations are almost negligibly affected by the vortex structures. In particular, Ortmanns & Kähler state that the jet-boundary-layer interaction produced less turbulent fluctuations when compared to a free-jet flow. This is an important finding for the interpretations of results from experiments and computations. They conclude, similar to Barth *et al.* (2011) but in total contrast to Zhang (2003), that only the large-scale momentum transport was the origin of the mixing processes in the flow. Ortmanns (2008) and Mahmood & Radespiel (2009, 2011) investigated experimentally and computationally, respectively, the single round VGJ setup from Ortmanns & Kähler (2007). Ortmanns (2008) claimed that a fully-developed vortex was obtained for $\alpha = 45°$ and $\beta = 90°$ to $105°$, but that a smaller pitch angle $\alpha = 30°$ increased the overall flow-separation control performance. Ortmanns could show that increasing λ increased the vortex core wall-normal distance and radius in agreement with Zhang & Collins (1997). Moreover, Ortmanns (2008) showed that the vortex circulation was linearly dependent on λ.

CHAPTER 3

Governing Equations

This thesis covers to a large extent the concept, development and evaluation of statistical models for passive VVGs and active VGJs, complemented with computational investigations of fully-resolved flow-control devices. The computational investigations that are presented in this work rely on the RANS equations and therefore, a brief introduction of the governing flow equations is presented in this section. The incompressible turbulent flow is governed by the continuity equation and the Navier-Stokes equations that read

$$\frac{\partial u_i}{\partial x_i} = 0, \tag{3.1}$$

$$\frac{\partial u_i}{\partial t} + u_j \frac{\partial u_i}{\partial x_j} = -\frac{1}{\rho}\frac{\partial p}{\partial x_i} + \frac{\partial}{\partial x_j}(2\nu s_{ij}), \tag{3.2}$$

with u_i and p as the instantaneous velocity and pressure fields, ρ and ν as the constant density and the kinematic viscosity, respectively. The instantaneous strain-rate tensor is denoted as $s_{ij} \equiv (u_{i,j}+u_{j,i})/2$. The strength of these equations is that they take all turbulence effects into account, from the smallest Kolmogorov scales up to the largest geometric flow scales. A direct-numerical solution (DNS) of equations (3.1) and (3.2) normally leads to an enormous amount of computational effort and thus, costs. Research is then mostly restricted to simple geometries and low-to-moderate Reynolds numbers, and thus has limited applicability for most engineering applications which often involve high Reynolds number turbulent flows. Therefore, statistical approaches are widely used, and the instantaneous flow-field variables are, for this purpose, decomposed into mean and fluctuating parts. The mean part is usually defined as the ensemble-average value over a large set of realizations, whereas the property of the fluctuating part is the vanishing ensemble-averaged value. According to this decomposition, see for example Pope (2000), the instantaneous velocity and pressure from equations (3.1) and (3.2) become

$$u_i = U_i + u_i', \tag{3.3}$$

$$p = P + p', \tag{3.4}$$

denoting capital-letter quantities as the mean parts, and small-letter quantities with primes as the fluctuating parts. From the above definition of the

decomposition, it follows that the ensemble-averaged equations (3.3) and (3.4) read

$$\overline{u_i} \equiv U_i, \qquad \overline{u_i'} = 0, \tag{3.5}$$

and

$$\overline{p} \equiv P, \qquad \overline{p'} = 0. \tag{3.6}$$

The decomposition of the instantaneous flow-field variables into a mean and a fluctuating part in equations (3.3) and (3.4) is commonly known as "Reynolds decomposition". Applying the Reynolds decomposition, i.e., plugging equations (3.3) and (3.4) into equations (3.1) and (3.2), followed by an ensemble-averaging yields the incompressible RANS mean-flow equations:

$$\frac{\partial U_i}{\partial x_i} = 0, \tag{3.7}$$

$$\frac{\partial U_i}{\partial t} + U_j \frac{\partial U_i}{\partial x_j} = -\frac{1}{\rho}\frac{\partial P}{\partial x_i} + \frac{\partial}{\partial x_j}(2\nu S_{ij} - \overline{u_i' u_j'}), \tag{3.8}$$

where $S_{ij} \equiv (U_{i,j} + U_{j,i})/2$ defines the mean strain-rate tensor. By applying the Reynolds decomposition and multiplying equation (3.2) with the density ρ, the mean-flow momentum equation in equation (3.8) gains an additional turbulence-stress term $-\rho\overline{u_i' u_j'}$ on the right-hand side, known as the "Reynolds-stress tensor". It represents the additional internal turbulence stresses that emerge due to the velocity fluctuations and that act on the mean flow.

An equation for the Reynolds-stress tensor $-\rho\overline{u_i' u_j'}$ can be derived from the Navier-Stokes equations, but the problem lies in the generation of even higher-order moments like $\overline{u_i' u_j' u_k'}$. This is commonly called the "closure problem" of turbulence. Turbulence modelling is the art of finding additional equations for the Reynolds-stress term to close the system of equations, and to make it solvable. The aim is therefore to design a closed system of equations for the one-point quantities U_i, P and $\overline{u_i' u_j'}$. Therefore, the Reynolds-stress term needs to be modelled, containing only known quantities. The modelling of the Reynolds-stress tensor fills numerous books as well as journal papers, and is not part of this work and therefore not presented. From the existing modelling approaches, the concept of the differential Reynolds-stress model (DRSM) and the provision of transport equations for the individual tensor components is suitable for capturing their time and spatial development.

The Reynolds-stress-tensor transport equation is derived by means of subtracting equation (3.8) for the mean velocity U_i from equation (3.2) for the instantaneous velocity u_i. The resulting equation for $u_i' = u_i - U_i$ is then multiplied by u_j', and combined with the corresponding equation with switched i and j indices. After averaging, we get

$$\frac{D\overline{u_i' u_j'}}{Dt} = \mathcal{P}_{ij} - \epsilon_{ij} + \Pi_{ij} + \mathcal{D}_{ij}. \tag{3.9}$$

The terms on the right-hand side of equation (3.9) represent the turbulence production tensor $\mathcal{P}_{ij}$, the dissipation-rate tensor ϵ_{ij}, the pressure strain-rate tensor Π_{ij}, and the turbulence diffusion $\mathcal{D}_{ij}$, respectively. Turbulence modelling is needed for the latter three terms, whereas the production tensor $\mathcal{P}_{ij}$ is explicitly given if $\overline{u_i' u_j'}$ is known:

$$\mathcal{P}_{ij} \equiv -\overline{u_i' u_k'} \frac{\partial U_j}{\partial x_k} - \overline{u_j' u_k'} \frac{\partial U_i}{\partial x_k}, \tag{3.10}$$

and rotational mean-flow effects enter equation (3.10) naturally, providing a major advantage over, for example, simpler eddy-viscosity models. As stated before, the remaining three terms on the right-hand side in equation (3.9) need to be modelled, where the major challenge lies on the model for the redistributive pressure strain-rate tensor Π_{ij}, leading to various DRSM approaches in the literature. The interested reader is referred to relevant text books on the topic; see for example Wilcox (1988), or Pope (2000). The concept of the statistical VG modelling approach, which is based on the transport equation for $\overline{u_i' u_j'}$ and an extension for the Reynolds-stress tensor, is described in detail in section 4.3.

CHAPTER 4

Vortex Generator Modelling

4.1. Existing Vane Vortex Generator Models

Since the inclusion of VGs in a computational mesh is a rather cumbersome and time-consuming procedure, several research teams have developed models for passive VVGs in order to circumvent these difficulties. To my knowledge, the first work on VVG modelling, which is fully-integrated in a Navier-Stokes solver, was published by Bender *et al.* (1999) and is referred to as the Bender-Anderson-Yagle (BAY) VVG model in this thesis. As Bender *et al.* point out, only "the large-scale effects induced on the secondary flow by the vortex generators are of interest" for the designer of fluid-mechanical systems that use VVGs. A modelling approach that solely takes these large-scale effects into account is therefore assumed to be sufficient to model VVGs with much less computational effort and time. The BAY model is based on relations between the local flow-field primitive parameters and the geometrical-setup parameters of the VVG and it uses volume side lift forces $\mathbf{L_i}$ which substitute the resolved VVG geometries in a computational grid. The volume forces $\mathbf{L_i}$, which describe the lift that originates from the modelled VVGs, are based on the lifting-line theory (LLT) by Prandtl (1921). The modelled forces are then applied on chosen cells V_i in the computational mesh. They represent the influence region of the modelled VVGs, and act perpendicular to the freestream and parallel to the wall. The volume cells V_i, which represent the forcing region for the BAY model, need to be specified manually. Therefore, the cell coarseness, and the fineness of the VVG-covering grid is given by the user. In particular, Bender *et al.* (1999) report the option to include $\mathbf{L_i}$ in small clustered cell regions for isolated VVGs, up to an entire spanwise field of cells for a tight array of VVGs with a small spanwise symmetry distance D. It is mentioned that the BAY model also includes an empirical calibration constant c_{BAY}. Bender *et al.* describe a dependency of results on the total number of grid cells $\Sigma V_i = V_M$that represent the modelled VVGs (linear mode), as well as a dependency on the absolute value of c_{BAY} (asymptotic mode).

Dudek (2011) implemented the BAY model into the Wind-US Navier-Stokes solver, and could achieve good results when compared to fully-gridded VVG data and to experiments for a single VVG in a subsonic ZPG boundary layer, for a VVG array in a circular S-duct, and for counter-rotating VVG pairs in supersonic boundary-layer flow.

Jirásek (2005) presented a further development of the BAY model, calling it jBAY model. The proposal removes the need for user inputs regarding the definition of the cell volumes V_i that contain the original resolved VVG structures. Using the original BAY model could be cumbersome because VVGs can be very thin structures and it might be difficult to define the correct volume cells V_i. The dependency on the constant c_{BAY} may also involve further difficulties in obtaining a reliable model setup. VVG arrays in the original BAY model asymptotic mode are regarded as one large single VVG which covers the corresponding spanwise domain. The force $\mathbf{L_i}$ is applied on each grid point which is included in the volume for the modelled "single" VVG. For the case of VVG arrays, Jirásek (2005), in contrast to Bender *et al.* (1999), suggests the jBAY model that applies a spanwise-distributed lift force $\mathbf{L_i}$ on specific grid points. For that, the VVGs are considered to be infinitely thin structures which cut the mesh cells and edges, creating new grid points at intersections. The resulting volume force is projected to only these newly created grid points to reduce the application of the lifting-force terms. Jirásek tested the jBAY model with a universal constant $c_{\mathrm{BAY}} = 10$ on three different cases and achieved excellent agreement of results when compared to fully-resolved VVG computations and experimental data. Therefore, the uncertainties connected to the original BAY model was removed by the jBAY model. Still, the flow structures downstream of the VVG forcing plane need to be resolved properly in order to achieve good results.

Wendt (2004) presented an emprical VVG model approach by means of a parameterization study for passive VVGs. Wendt carried out his research in a straight pipe turbulent boundary layer with VVGs either mounted in a single configuration or, in case of arrays, evenly distributed along a circumferential row at a constant streamwise position. The arrays investigated were both of corotating and of counter-rotating (including common-flow-down/up settings) types. His results cover an extensive study of the geometrical VVG setup as well as the general flow setup. It was shown that counter-rotating VVG arrays performed better when compared to a single VVG and found out that a corotating setup gave poorer results than a single VVG. Wendt used his results as a basis for developing a VVG model. By using the Lamb-Oseen vortex model and the LLT, he was able to model the streamwise peak vorticity ω_z and the vortex circulation Γ. The model results presented by Wendt (2004) show a very good agreement when compared to experiments with single VVGs.

Dudek (2006) implemented Wendt's model into the Wind-US Navier-Stokes solver. She evaluated Wendt's VVG model by means of VVG arrays in several different flow cases. The model results were compared to results from fully-resolved VVG computations and to experimental results. The conclusion of her work was that the empirical VVG model generated overall satisfactory results and could confirm the findings of Wendt (2004).

Another approach was presented by Gleyzes & Pailhas (2011), who have used the original BAY model for a triangular passive VVG to mimic an active

VGJ. Therefore, they had to find reasonable parameter values for the BAY-modelled VVG that created a comparable vortex from a VGJ. Whereas the VGJ actuator's setup was amongst others defined by $\alpha = 30°$, and the BAY-modelled equivalent VVG was found to give comparable results for an angle of incidence $\alpha = 45°$. Near-field data show differences in results due to the different vortex generation by VVGs and VGJs. Nevertheless, results in the far field show a fairly good agreement between the BAY-modelled VVGs, experiments, as well as computations with fully-gridded VGJs. Finally, Gleyzes & Pailhas (2011) state that there is no high sensitivity of the BAY model results for a VVG-α-range of $\pm 15°$ at such high α as 45°. In total, they experienced heavily reduced global CPU time, especially when taking the parameter variation study into account, and showed that the BAY model for passive VVGs could in principle be used for an analysis of active VGJs.

4.2. User Challenges of VG Models

The expression "VG modelling" already implies that the flow physics, which is predominating in such fluidic flows, is not realisticly captured. Instead, a general modelling approach reduces the physical description in such a way that results become satisfactory with the benefits of simpler preprocessing and reduced CPU time. Furthermore, VG models are used in combination with RANS turbulence models that already model the mean-flow characteristics and properties, and this reduces result accuracy per se. Moreover, VG modelling results strongly depend on the specific modelling concept. This could be observed in the foregoing section where the VVG model results from different sources have been compared to either experiments, and/or fully-resolved VVG computations. These approximated results have shown to be often very sactisfactory for the presented cases. Nevertheless, it remains unclear if the introduced VVG models could be able to predict different, or even more complicated flows, as well as a wide setup-parameter range reasonably correct. Unfortunately, the user of such VG models can never be totally confident about the computational results, at least unless a certain experience for the specific VG model and/or reference data from corresponding experiments exist. The long-term goal of VG modelling research is to elimante the latter issue, giving the user a more or less universal tool for a-priori-analyses of applied flow-separation control.

On the other hand, VG models involve many advantages in a computational analysis as mentioned previously. Parameter variations become less time-consuming due to reduced preprocessing complexity, as well as heavily reduced total computer processing times. Moreover, computational analyses using the same VG model make it possible to draw conclusions regarding the relative change in results, enabling the determination of trends and tendencies when setup parameters change.

4.3. Statistical Vortex Generator Models

This thesis deals mainly with two different statistical VG model approaches for passive and active flow-separation control. The two VG models are based on the formation of so-called additional vortex stresses that originate from the vortices. Before it is possible to determine these stresses, the vortex velocities that represent the actual generated vortices need to be modelled first. For that, a vortex model is required that makes it possible to analytically determine the vortex velocities for a specific VG setup. The Lamb-Oseen vortex model is used in this thesis, and it contains the following parameters: the vortex circulation $\Gamma_{\max}$, the viscous core radius r_0, and the vortex core location (h_c/z_c). Based on the modelled vortex velocities, their spanwise-averaged second-order statistics, reading $\overline{V_iV_j}(y,z)$, can be determined. As a result, the $\overline{V_iV_j}(y,z)$ tensor can be used as an additional forcing term in the RANS momentum equation.

The principle difference between the VVG and the VGJ models, that are presented in the following sections, is the ansatz for the determination of the Lamb-Oseen vortex-model input paramaters $\Gamma_{\max}$ and r_0, because VVGs and VGJs generate vortices in different ways. In this section, it is explained how the total vortex-velocity field $V_i(y,z)$ for a spanwise modelled VG array with a large number of VGs is treated in the turbulence description of a computational analysis, and how the additional vortex stress tensor is formed and finally added to the Reynolds-stress tensor.

4.3.1. *Lamb-Oseen Vortex Model*

The Lamb-Oseen vortex model was chosen for the statistical-modelling approach for passive VVGs and active VGJs since it has shown to model the cross-plane components $[V_y, V_z](y,z)$ for streamwise vortices reasonably well. The resulting vortex-velocity field in the radial direction reads

$$V_\Phi(r) = \frac{\Gamma_{\max}}{2\pi r}\left[1 - e^{-\left(\frac{r}{r_0}\right)^2}\right], \tag{4.1}$$

with $\Gamma_{\max}$ for the vortex circulation, r_0 for the vortex core radius, and $r = \sqrt{(y-h_c)^2 + (z-z_c)^2}$ is the radial distance from the vortex core (h_c, z_c) in cartesian coordinates. As mentioned previoulsy, the two different VG models for passive VVGs and for active VGJs require different ansatzes for $\Gamma_{\max}$, r_0 and (h_c, z_c). The details about how the specific vortex-model parameters are determined are given in sections 4.4 and 4.5.

After determining $\Gamma_{\max}$, r_0 and h_c, the resulting induced VG array velocity field $V_i(y,z)$ is identified by means of a superposition of each single vortex-velocity field $V_\Phi(r)$ and its corresponding mirror image; see also figure 4.1. In order to obtain the additional turbulent vortex stresses for the statistical VG models, the induced velocity field $V_i(y,z)$ is split into its velocity components $V_y(y,z)$ and $V_z(y,z)$ in the wall-normal and the spanwise direction, respectively ($V_x = 0$ due to the choice of the two-dimensional Lamb-Oseen vortex model).

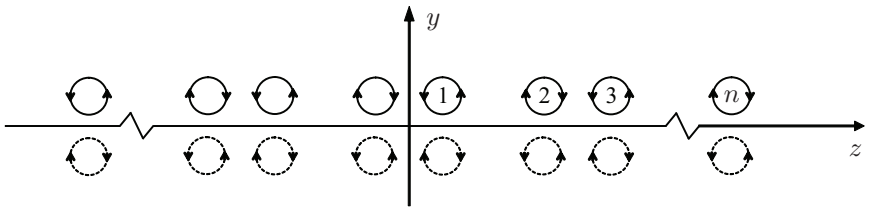

FIGURE 4.1. VG model forcing plane: vortex array with n VG pairs and mirror images for the analysis of the superimposed vortex-velocity field $V_i(y, z)$ from equation (4.2). [Image inspired by Törnblom & Johansson (2007).]

According to Törnblom & Johansson (2007), the velocity components for a counter-rotating common-flow-down VG array setup read

$$[V_x, V_y, V_z](y, z) = \sum_{n=1}^{\infty}(-1)^{n+1} \sum_{m=1}^{4}(-1)^{m+1} \frac{V_\Phi(r_m)}{r_m}[0, \Delta z_m, -\Delta y_m], \quad (4.2)$$

where

$$r_m = \sqrt{\Delta y_m^2 + \Delta z_m^2}, \quad (4.3)$$

and

$$\begin{aligned} \Delta y_1 &= y - h_n, \quad & \Delta z_1 &= z - z_n, \\ \Delta y_2 &= y + h_n, \quad & \Delta z_2 &= z - z_n, \\ \Delta y_3 &= y + h_n, \quad & \Delta z_3 &= z + z_n, \\ \Delta y_4 &= y - h_n, \quad & \Delta z_4 &= z + z_n. \end{aligned} \quad (4.4)$$

The spanwise-averaged second-order statistics of the total additional vortex velocities $V_i(y, z)$ from equation (4.2) can now be determined and are assumed to act as additional turbulent vortex stresses within the statistical VG model ansatz and can then be added to the mean-flow turbulence; see section 4.3.3.

4.3.2. *Velocity Triple Decomposition*

The concept of the velocity triple decomposition makes it possible to formally add the additional total vortex-velocity field $V_i(y, z)$ from equation (4.2) to the mean-flow velocity U_i and the turbulent fluctuations u_i' from equation (3.5):

$$u_i(x, y, z, t) = U_i(y) + u_i'(x, y, z, t) + V_i(y, z). \quad (4.5)$$

The additional total velcocity field V_i can now, for example, be added to the mean flow U_i in a RANS computation. This resolves the mean-flow velocity U_i and the generated vortices V_i, thus only expressing the turbulent part u_i' by a conventional turbulence model. On the other hand, it is possible to solely resolve the mean-flow velocity U_i, and instead to add V_i to the turbulent fluctuations u_i' and thereby, treat the combination $u_i' + V_i$ in a turbulence

model. The two approaches perform differently in a computational analysis. The first one resolves the VGs and the generated vortices downstream of the VGs which requires a fully-resolved three-dimensional computational grid. This makes the first approach and its results highly grid dependent. The second proposal adds the additional vortex velocities within the turbulence model and, by that, a computational analysis may reduce to two-dimensional computational grids only. As a consequence, the results including the vortices become solely dependent on the turbulence model used. Still, the VG forcing plane[1], where the statistical vortex-stress terms are applied, needs to be adequately resolved in order to capture the modelled vortices within the turbulence model. The ansatz for adding V_i to u_i' within a statistical turbulence model is used for the statistical VG modelling approaches in this thesis, and the combined velocity field v_i' from the turbulence fluctuations u_i' and the vortex veloities V_i is defined as

$$v_i'(y,z,t) \equiv u_i'(y,z,t) + V_i(y,z). \tag{4.6}$$

It is now possible to form the time- and spanwise-averaged second-order statistics of $v_i'(y,z,t)$ which, in turn, are used for a substitution of the original Reynolds-stress tensor by an extended Reynolds-stress tensor $\overline{v_i'v_j'}(y)$ which includes the modelled vortex stresses from $V_i(y,z)$.

4.3.3. *Extended Reynolds Stress Tensor*

As briefly mentioned in section 4.3.2, the concept of the statistical vortex modelling is to assume that the spanwise-averaged second-order statistics of the additional vortex-velocity field $V_i(y,z)$ from equation (4.2) act as additional stresses on the mean flow. By making this explicit assumption, the additional spanwise-averaged second-order statistics of the vortex-velocity field $V_i(y,z)$, or simply the vortex stresses, enter the DRSM equations through the combined stress tensor $-\rho\overline{v_i'v_j'}(y)$ for $v_i'(y,z,t)$ from equation (4.6). This substitutes the Reynolds-stress tensor $-\rho\overline{u_i'u_j'}(y)$ with the extended Reynolds-stress tensor for the combined stresses $-\rho\overline{v_i'v_j'}$, where

$$\begin{aligned} -\rho\overline{v_i'v_j'}(y) &= -\rho\overline{(u_i'+V_i)(u_j'+V_j)}, \\ &= -\rho\left[\overline{u_i'u_j'}(y) + \Delta\overline{u_i'u_j'}(y)\right], \end{aligned} \tag{4.7}$$

and

$$\Delta\overline{u_i'u_j'}(y) \equiv \overline{V_iV_j}(y). \tag{4.8}$$

[1]The term "forcing plane" is generally used in this thesis and denotes the plane normal to the freestream direction, and at the VG array position. Strictly valid only in three dimensions, the VG forcing plane reduces to a VG forcing line in two-dimensional flows.

The cross-product terms in equation (4.7) form the correlations $\overline{u_i' V_j}$ and $\overline{u_j' V_i}$. These contributions become zero, because their mean values are derived from a spanwise- and time-averaging of $u_j' V_i$, and because the velocity field $V_i(y,z)$ is steady. The additional vortex stresses[2] can be determined from the spanwise-average term

$$\Delta\overline{u_i' u_j'}(y) = \frac{1}{D}\int_{-D/2}^{D/2} V_i(y,z) V_j(y,z) dz. \tag{4.9}$$

where the vortex-velocity field is given by equation (4.2). It is sufficient to integrate and spanwise-average the second-order statistics in equation (4.9) over a distance D since the vortex-velocity field $V_i(y,z)$ is periodic in the spanwise direction. Additional contributions $\Delta\overline{u_i' u_j'}(y)$ are, due to the choice of the Lamb-Oseen vortex model ($V_x = 0$), only nonzero for $\Delta\overline{v'v'}(y)$ and $\Delta\overline{w'w'}(y)$. Moreover, a wall-damping function, $[1 - \exp(-20y/h)]$, is introduced and applied on equation (4.9), because the spanwise vortex-velocity component $V_z(y,z)$ at the wall boundary does not cancel out and would result in a finite value for $\Delta\overline{w'w'}(y = 0)$.

In that way, a summation of the boundary-layer turbulence stresses $\overline{u_i' u_j'}(y)$ with the VG model vortex stresses $\Delta\overline{u_i' u_j'}(y)$ can be carried out. The vortex stresses $\Delta\overline{u_i' u_j'}(y)$ are thereby applied at the VG forcing plane, and from there, they influence the downstream development of the mean flow. The VVG model forcing plane is defined as the location of the vane trailing edge where the generated vortices detach. In terms of the VGJ model, the location of the jet exit center is defined as the VGJ forcing plane.

As described in chapter 3, a DRSM is suitable to properly describe the streamwise transport and development of the individual components of $\overline{u_i' u_j'}(y) + \Delta\overline{u_i' u_j'}(y)$. Furthermore and unlike simpler turbulence models, a DRSM enables to account for the energy transfer between the different components of the extended Reynolds-stress tensor $\overline{v_i' v_j'}(y)$. In particular, the vortex stress tensor $\Delta\overline{u_i' u_j'}(y)$ does not enable the normal and the important shear stresses, $\Delta\overline{u'u'}(y)$ and $\Delta\overline{u'v'}(y)$, respectively, and their production is instead established through $\mathcal{P}_{12} = \overline{v'v'}\frac{\partial V_x}{\partial y}$ in the transport equations for $\overline{u_i' u_j'}(y) + \Delta\overline{u_i' u_j'}(y)$ within the DRSM.

4.4. Statistical Vane Vortex Generator Model

The original statistical VVG model was initially proposed by Törnblom & Johansson (2007), and it is presented in this section. As mentioned in section 4.3.1, the values for $\Gamma_{\max}$, r_0, and (h_c, z_c) need to be determined with respect to the VG model used. The spanwise vortex core location z_c, which is initially a function of the VVG setup parameters d and D, as well as d and D must be

[2]From here on, the factor $-\rho$ is obmitted for better readability. Still, the term "stresses" is used for the remaining tensor.

explicitely given by the user in order to determine the total vortex-velocity field for VVG arrays from equation (4.4). Furthermore, empirical well-established values for r_0 and h_c enter the VVG model with $r_0 = 0.1h_{VG}$ according to Törnblom & Johansson (2007), and $h_c = h_{VG}$ due to the distinct vortex shedding from the VVGs.

The central ansatz for the VVG model are very thin vanes which can be considered as small wings, mounted normal on the control surface; see also figures 1.1 and 2.2. The LLT is used for the determination of $\Gamma(y)$ across the vane, and thereby, the maximum value Γ_{max}. The spanwise circulation distribution $\Gamma(y)$ across a wing along the spanwise coordinate y is given by

$$\Gamma(y) = \frac{K}{2} U(y) c(y) \left[\alpha(y) - \frac{w(y)}{U(y)} \right], \tag{4.10}$$

where $U(y)$ represents the incoming velocity distribution across the wing, $c(y)$ the wing chord distribution, K the local section lift slope of the wing at zero angle of attack, and $w(y)$ the downwash-velocity distribution

$$w(y) = \frac{1}{4\pi} \int_{-h}^{h} \frac{d\Gamma}{dy'} \frac{1}{y' - y'_0} dy'. \tag{4.11}$$

The term in squared brackets in equation (4.10) specifies the effective angle of attack

$$\alpha_{\text{eff}}(y) \equiv \alpha(y) - \frac{w(y)}{U(y)}, \tag{4.12}$$

which develops due to the finite wing aspect ratio. The LLT strictly holds only for high-aspect-ratio wings for small angles of attack α in inviscid free-flight conditions. By means of modelling $\Gamma(y)$ for relatively small vanes that are mounted in a boundary-layer flow, some of its assumptions are not strictly valid as a result of: 1) a spanwise varying boundary-layer velocity profile $U(y)$ instead of a constant freestream velocity U_∞; 2) VVGs being wing-like vanes with very low aspect ratios; 3) possible neighbouring-vortex interaction; and 4) a rather high vane angle of incidence α towards the mean-flow direction. Therefore, the LLT should only be considered as an approximation to estimate the circulation distribution $\Gamma(y)$ across the vane. The circulation Γ_{max} is then used as an input parameter to the Lamb-Oseen vortex model from equation (4.1). A solution method for equations (4.10) and (4.11) is given in the next section.

4.4.1. *Solution Method for the Lifting-Line Theory*

In a next step on the way to model VVGs, it is necessary to solve equations (4.10) and (4.11) numerically by means of a Fourier series; see Glauert (1926). A suitable transformation for the y-coordinate of a single vane and its mirror image is given by

$$y(\theta) = -h_{VG} \cos(\theta), \tag{4.13}$$

with $0 \leq \theta \leq \pi$ as the new y-coordinate limits. The Fourier-series ansatz for equation (4.10) according to Glauert (1926) reads

$$\Gamma(\theta) = 4h_{\mathrm{VG}}U_{\mathrm{ref}} \sum_{n=1}^{\infty} A_n \sin(n\theta). \tag{4.14}$$

The induced downwash $w(\theta)$ from equation (4.11) at a certain spanwise position θ in combination with equation (4.13) becomes

$$\begin{aligned} \frac{w(\theta)}{U_{\mathrm{ref}}} &= \frac{1}{4\pi} \int_0^{\pi} \frac{d\Gamma(\theta')}{d\theta'} \frac{d\theta'}{\cos\theta' - \cos\theta}, \\ &= \frac{1}{\pi} \int_0^{\pi} \frac{\sum_{n=1}^{\infty} nA_n \cos(n\theta')}{\cos\theta' - \cos\theta} d\theta', \\ &= \sum_{n=1}^{\infty} nA_n \frac{\sin(n\theta)}{\sin\theta}, \end{aligned} \tag{4.15}$$

where the standard integral

$$\int_0^{\pi} \frac{\cos(n\theta')\, d\theta'}{\cos\theta' - \cos\theta} = \frac{\pi \sin(n\theta)}{\sin\theta} \tag{4.16}$$

is used. Equations (4.14) and (4.15) are plugged into equation (4.10), leading to the system of equations

$$\sum_{n=1}^{\infty} A_n \sin(n\theta)(\mu(\theta)n + \sin\theta) = \mu(\theta) \frac{U(\theta)}{U_{\mathrm{ref}}} \alpha(\theta) \sin\theta, \tag{4.17}$$

where $\mu(\theta) = Kc(\theta)/8h_{\mathrm{VG}}$. This system of equations is solved by a truncation of the series at $n = N$ colloation points for the vane and its mirror image, and solving at $M = (N-1)/2$ collocation points for the vane only, viz. $0 \leq y \leq h_{\mathrm{VG}}$ and $\frac{\pi}{2} \leq \theta \leq \pi$, respectively. The solution for A_n is then used to solve the circulation distribution $\Gamma(y)$ across the vane.

4.4.2. *Original Statistical Vane Vortex Generator Model*

When the circulation distribution $\Gamma(y)$ and its maximum value Γ_{max} are determined, the vortex velocities $V_i(y, z)$ from equations (4.1) and (4.2) and the vortex stresses $\Delta\overline{u_i'u_j'}(y)$ from equation (4.9) can be formed and added to the turbulence stresses $\overline{u_i'u_j'}(y)$ at the VVG forcing plane.

A typical distribution of the turbulence stresses $\overline{u_i'u_j'}(y)$ for a ZPG boundary-layer flat-plate flow is given in figure 4.2. The additional vortex stresses $\Delta\overline{v'v'}(y)$ and $\Delta\overline{w'w'}(y)$ for a specific VVG setup, see figure 4.3, are then added to the turbulence stresses, resulting in the combined stresses in figure 4.4. These represent the combined stresses of the extended Reynolds-stress tensor which is treated by the transport equation of a DRSM turbulence model.

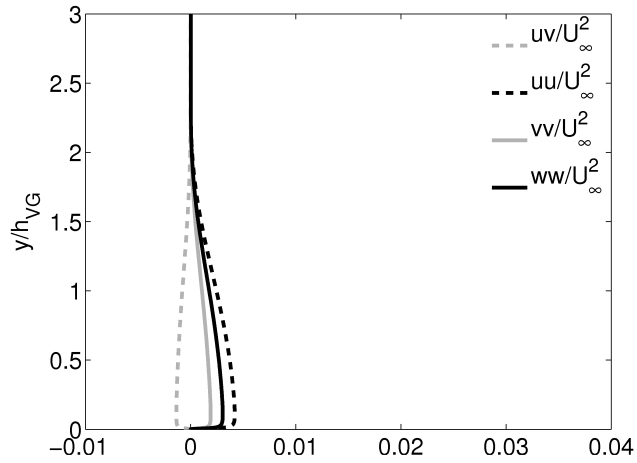

FIGURE 4.2. Nondimensional boundary-layer turbulence stresses at the VVG model forcing plane.

4.4.3. *Improvement of the Statistical Vane Vortex Generator Model*

Since the original proposal of the VVG model by Törnblom & Johansson (2007) did not account for the vortex-stress components $\Delta\overline{u'u'}(y)$ and $\Delta\overline{u'v'}(y)$, an improved VVG model is proposed on the basis of the original VVG model. A straightforward way to include also those correlations which contain products of u' seems to simply extend the Lamb-Oseen vortex model by a streamwise-velocity component V_x. The $\Delta\overline{u'u'}(y)$ component could be derived from this

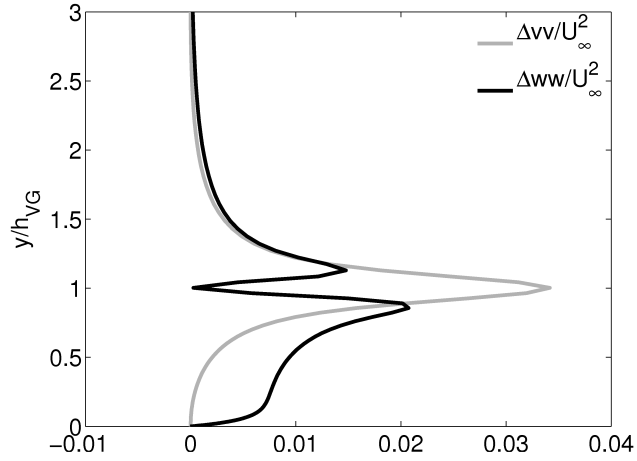

FIGURE 4.3. Nondimensional additional vortex stresses at the VVG model forcing plane. $U_\infty = \mathbf{26.5\ m/s}$, $\alpha = \pm\mathbf{15}^\circ$, $h_{\mathrm{VG}}/\delta_{99} = \mathbf{0.65}$.

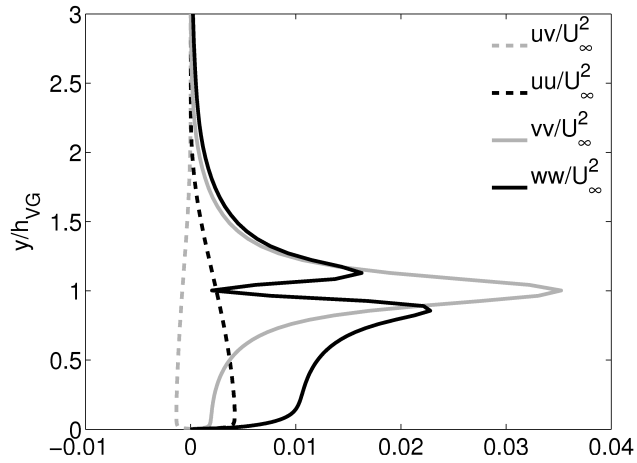

FIGURE 4.4. Nondimensional combined stresses, summation of the boundary-layer turbulence stresses from figure 4.2 and the additional vortex stresses from figure 4.3.

ansatz but not $\Delta\overline{u'v'}(y)$, because any streamwise vortex-velocity component V_x would not be correlated with the cross-plane vortex-velocity components V_y and V_z. Therefore, another approach for modelling both the $\Delta\overline{u'u'}(y)$ and the $\Delta\overline{u'v'}(y)$ is proposed here. The existing vortex-stress components $\Delta\overline{v'v'}(y)$ and $\Delta\overline{w'w'}(y)$ are used in order to model the remaining nonzero vortex-stress components $\Delta\overline{u'u'}(y)$ and $\Delta\overline{u'v'}(y)$. Also the mean strain-rate tensor S_{ij} is included in this ansatz and it accounts for the effects of the velocity gradient $\partial U(y)/\partial y$ in the boundary layer, with S_{ij} becoming zero at the boundary-layer edge. Thereby, it is ensured that the additional modelled vortex stresses become zero when the local boundary-layer edge is reached. The suggested $\Delta\overline{u'u'}(y)$ and $\Delta\overline{u'v'}(y)$ stresses read

$$\begin{aligned}\Delta\overline{u'u'}(y) &= C_{uu}\cdot S(y)\frac{r_0^2}{\Gamma_{\max}}\left[\Delta\overline{v'v'}(y)+\Delta\overline{w'w'}(y)\right],\\ \Delta\overline{u'v'}(y) &= -C_{uv}\cdot S(y)\frac{r_0^2}{\Gamma_{\max}}\left[\Delta\overline{v'v'}(y)+\Delta\overline{w'w'}(y)\right],\end{aligned}\tag{4.18}$$

where C_{uu} and C_{uv} denote nondimensional constants in order to account for the correct amplitude of the modelled stresses. The constants C_{uu} and C_{uv} were determined empirically by means of examining the improved VVG model in ZPG flat-plate boundary-layer flow, as well as a comparison against experimental data and resolved computations, and read

$$\begin{aligned}C_{uu} &= 160,\\ C_{uv} &= 80.\end{aligned}\tag{4.19}$$

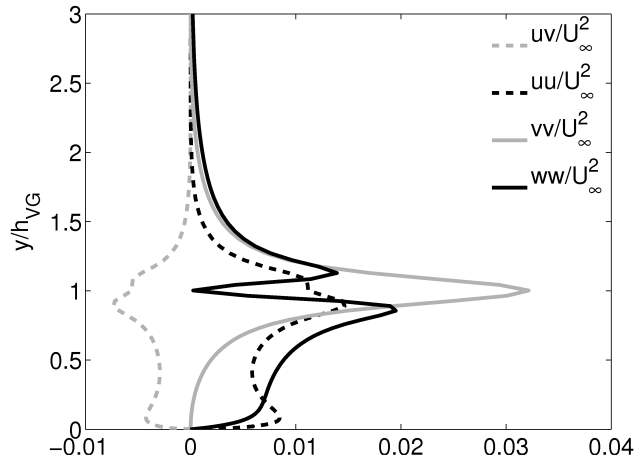

FIGURE 4.5. Nondimensional combined stresses for the improved VVG model at the VVG model forcing plane. $U_\infty = \mathbf{26.5\ m/s}$, $\alpha = \pm\mathbf{15}°$, $h_{\mathrm{VG}}/\delta_{99} = \mathbf{0.65}$; see also figure 4.3.

An example of the additional improved VVG stresses from equation (4.18) is given in figure 4.5. It can be seen how the two additional vortex stress distributions are mirrored and amplified by the coefficients C_{uu} and C_{uv} around the y-axis, and how they combine the characteristics of the $\Delta\overline{v'v'}(y)$ and $\Delta\overline{w'w'}(y)$ stresses. This improved VVG model has shown to have a better impact on the near-field stress development and thus, provides improved flow-separation control when compared to the original VVG model.

4.5. Statistical Vortex Generator Jet Model

It was shown that the distinct vortices which detach from the trailing edge of the VVG vanes can be modelled by an analytical derivation of the circulation $\Gamma_{\max}$ using the established theory of lifting lines by Prandtl. This concept cannot be assumed for modelling of VGJs. A different way of vortex generation by VGJs needs to be considered, and this section presents the development of the concept for the derivation of $\Gamma_{\max}$ for the statistical VGJ model. The derivation of the Lamb-Oseen vortex-model parameters $\Gamma_{\max}$, r_0 and $(h_{\mathrm{c}}, z_{\mathrm{c}})$ for the statistical VGJ model is mainly based on experiments from Ortmanns (2008) for single VGJ. The determination of suitable values was carried out via a least-squares data fitting of the experimental $U_\Phi(r)$ and the Lamb-Oseen vortex velocities $V_\Phi(r)$:

$$\min_x \|[U_\Phi(r) - V_\Phi(r)]\|_2^2. \tag{4.20}$$

It could be shown that the Lamb-Oseen vortex model represents the single VGJ vortices reasonably well (see figure 4.6). More details concerning the parameterization of the experimental vortices can be found in section 5.4 and in

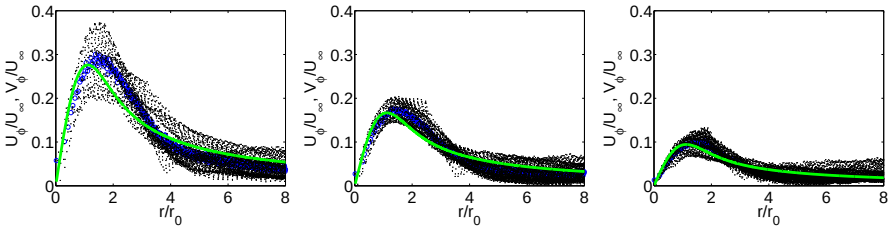

FIGURE 4.6. Nondimensional vortex velocity $U_\Phi(r/r_0)/U_\infty$ from experiments (dots), corresponding averaged values (circles), and the fitted vortex model $V_\Phi(r/r_0)/U_\infty$ (curve). Here: $U_\infty = \mathbf{25\ m/s}$, $\lambda = \mathbf{2.5}$, $\alpha = \mathbf{45}^\circ$, $\beta = \mathbf{90}^\circ$ at streamwise positions $x = 50$, 100, and 200 mm (from left to right).

appended Paper 3. Empirical values for r_0 and h_c and their dependencies on the VGJ setup parameters were derived from the parameterization of vortices from experiments. In contrast to the derivation of empirical values for r_0 and h_c, the vortex circulation Γ_{max} could be estimated from the the balance of the injected jet impulse and the added tangential momentum by an embedded boundary-layer vortex. This idealized model assumes a jet impulse $p_{VGJ} = F_{VGJ}\Delta t$ which is injected into the freestream during the time Δt into the boundary layer and that, in turn, creates a streamwise vortex when the jets deflects due to the mean boundary-layer flow. For the jet with a skew angle β, the magnitude of the momentum change p_{VGJ} can be estimated as

$$p_{VGJ} = F_{VGJ}\Delta t \sin\beta. \tag{4.21}$$

Due to the injected jet, the boundary layer experiences an increase of the cross-plane momentum by the fully-developed vortex. Likewise, the vortex momentum p_V of a fully-developed vortex which travels the streamwise distance x in Δt, see figure 4.7, reads

$$\begin{aligned} p_V &= \int_V \rho U_\Phi(r) dV_V, \\ &= \rho \Delta x 2\pi \int_0^R U_\Phi(r) r dr. \end{aligned} \tag{4.22}$$

As an evaluation of the experiments has shown, an upper integration boundary of $R = 5r_0$ is reasonable, because a circular area with $R = 5r_0$ contains most of the tangential vortex momentum. The injected jet impulse is suggested to be completely transformed, i.e., without any losses, into tangential vortex momentum. This balance enables the equation $p_{VGJ} = p_V$, which can be solved for Γ_{max} that enters equation (4.22) through the Lamb-Oseen vortex model. The expression for Γ_{max} is used to derive the modelled vortex velocities $V_i(y, z)$ for VGJs and enables the derivation of the vortex stresses for the

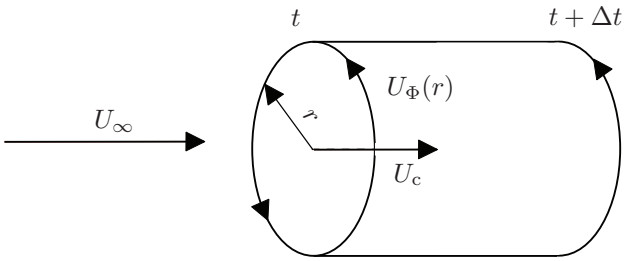

FIGURE 4.7. Schematic of a vortex tube of radius r and tangential velocity $U_\Phi(r)$ that travels the distance $\Delta x = U_c \Delta t$ during the time Δt.

statistical VGJ model. The Lamb-Oseen vortex model is then fully described by this ansatz, and the vortex model parameters read

$$\begin{aligned} \Gamma_{\max} &= C_\Gamma \sin\beta \left(\frac{\Phi_{\mathrm{VGJ}}^2 \lambda^2 U_\infty}{r_0} \right), \\ r_0 &= C_r \Phi_{\mathrm{VGJ}} \sqrt{\lambda}, \\ h_c &= C_h \Phi_{\mathrm{VGJ}} \lambda, \end{aligned} \tag{4.23}$$

where C_Γ, C_r and C_h represent suitable nondimensional vortex-model parameters for $\Gamma_{\max}$, r_0, and h_c. The numerical value of $C_\Gamma = \pi / \left[2\left(10 - \sqrt{\pi}\right)\right] \approx 0.2$ for $R = 5r_0$ in equation (4.22). The specific scaling for r_0 and h_c was empirically derived from the parameterization of the single-jet vortices from experiments by Ortmanns (2008). Universal nondimensional values are proposed to be C_r = 0.4 and C_h = 0.6 based on the results for $\alpha = 30$ °.

Vortex stresses for chosen VGJ settings at the VGJ forcing plane for C_Γ = 0.2, C_r = 0.4, C_h = 0.6 are given in figures 4.8 and 4.9. From the plots in figure 4.8, and a comparison with the corresponding VVG case in figure 4.3, it can be observed that the VGJ $\Delta\overline{v'v'}(y)$ peak stresses have decreased by ≈30%, whereas the VGJ $\Delta\overline{w'w'}(y)$ peak stresses have grown by a factor >2 when compared to the VVG model. This is the result of the small pitch angle α = 30° and the strong blowing perpendicular to the freestream direction for β = 90°, whereas VVG vortices enable a naturally stronger wall-normal component, and are also less affected by the presence of the wall. This is due to the fixed vortex core location at the VVG forcing plane which is in contrast to vortices originating from VGJs.

In the case for increasing λ (see figure 4.9), the general observation is that the vortex stresses are strongly amplified when compared to the lower λ-case. An increase in λ from 2.5 to 5.0 results in an increase for the $\Delta\overline{v'v'}(y)$ and the $\Delta\overline{w'w'}(y)$ peak stresses by a factor >4.5 and >8, respectively, essentially enabling similar peak stresses for both vortex stress components. The vortex core for λ = 5.0 is also located further away from the wall, compare with

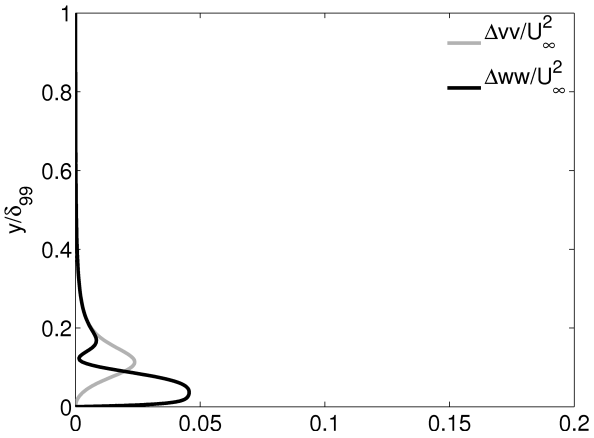

FIGURE 4.8. Nondimensional vortex-stress distributions at the VGJ model position from equation (4.23). $U_\infty = \mathbf{25\ m/s}$, $\lambda = \mathbf{2.5}$, $\Phi_{\mathrm{VGJ}}/\delta_{99} = \mathbf{0.07}$.

h_c in equation (4.23), and thereby enables, in combination with a relatively weaker-growing r_0, a stronger $\Delta\overline{v'v'}(y)$ due to the decreasing wall influence. The figures 4.8 and 4.9 generally show how the VGJ model reacts sensitively to a velocity ratio change in equation (4.23). Furthermore, it can be observed that the $\Delta\overline{v'v'}(y)$ stresses for the given VGJ setup become more than four times stronger when compared to the efficient VVG model configuration from figure 4.3, which probably leads to more efficient flow-separation prevention by VGJs.

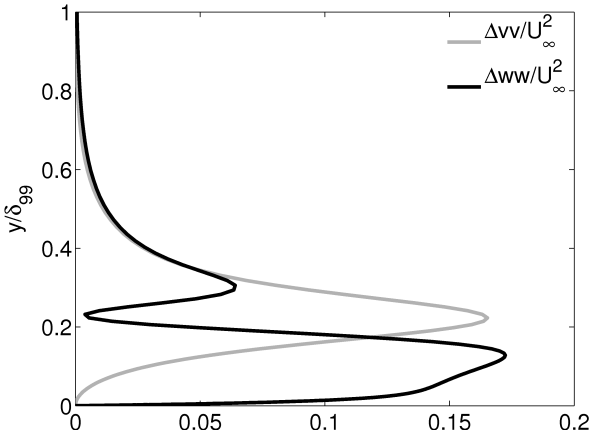

FIGURE 4.9. Nondimensional vortex-stress distributions at the VGJ model position from equation (4.23). $U_\infty = \mathbf{25\ m/s}$, $\lambda = \mathbf{5.0}$, $\Phi_{\mathrm{VGJ}}/\delta_{99} = \mathbf{0.07}$.

CHAPTER 5

Selected Results and Discussion

5.1. Original VVG Model in Adverse-Pressure-Gradient Flat-Plate Flow

The original VVG model was applied in APG flat-plate boundary-layer flow and evaluated against computations of a fully-gridded VVG array, as well as corresponding experiments by Lögdberg *et al.* (2010). A sensitivity study of the VVG model position dependency on skin-friction results was carried out.

The VVG array was installed in the APG section on a flat plate with a counter-rotating common-flow-down setup and consisted of rectangular vanes with $\alpha = \pm 15^\circ$. The local ratio of $h_{\mathrm{VG}}/\delta_{99} < 0.7$. In experiments and computations, a distinct separation bubble was present when no flow control was applied; see for example $c_f < 0$ in figure 5.1. Applying the fully-resolved VVGs, see the VG3D curve, the skin friction increased significantly and flow separation was prevented. The original VVG model, cf. the VG2D curve, showed a clear enhancement of the skin-friction, essentially preventing flow separation. Its impact on skin-friction increase was nonetheless not comparable to the VG3D computations.

In total, seven streamwise VVG forcing plane positions were examined, see also figure 5.2 for skin-friction results for $x_{\mathrm{VG}} \geq 1.25$ m. When the VVG model was applied at $x_{\mathrm{VG}} \leq 1.25$ m (not shown), the skin-friction distributions at the former separation-bubble location were increased for growing x_{VG}. For the $x_{\mathrm{VG}} \geq 1.25$ m plots in figure 5.2, the opposite effect was observed: the further downstream the VVG forcing plane, the weaker the impact on the mean flow. This led to a decreased skin-friction distribution and eventually, separated flow occured. A conclusion from this study is that there existed an optimum VVG position for flow-separation control using the original VVG model at the beginning of the APG section close to $x_{\mathrm{VG}} = 1.25$ m. Nevertheless, the overall flow state was rather insensitive on the VVG position. Still, a minimum distance between the model forcing plane and the originally separated region was required in order to eventually overcome flow separation.

5.2. Comparison of the VVG models

The original and the improved VVG models were evaluated and compared against each other, as well as against fully-resolved VVG computations and against experiments by Lögdberg *et al.* (2009, 2010). The VVGs were applied

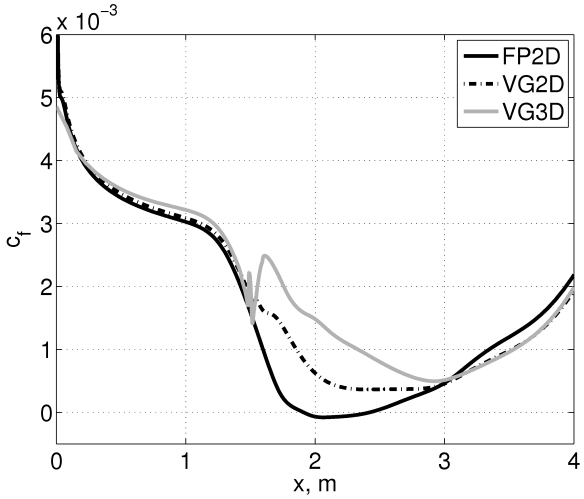

FIGURE 5.1. Local skin-friction coefficient distributions for computations without VVGs (FP2D), with the original VVG model (VG2D), and fully-gridded VVGs (VG3D). Here: baseline case for $x_{\mathrm{VG}} = 1.54$ m.

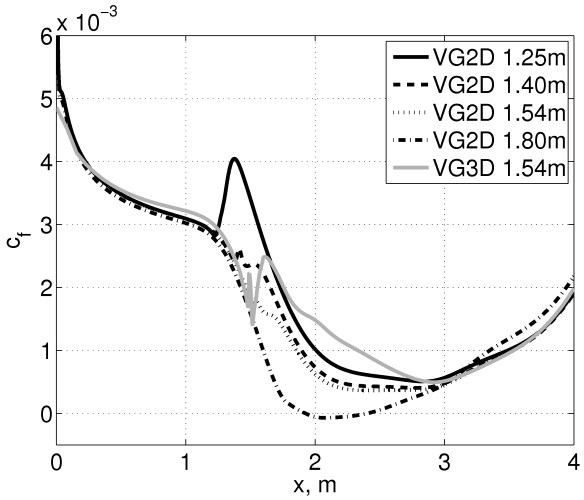

FIGURE 5.2. Local skin-friction coefficient distributions for a streamwise-position variation of the original VVG model forcing plane (VG2D) for 1.25 m $\leq x_{\mathrm{VG}} \leq$ 1.80 m. Results for the fully-resolved computations (VG3D) for the baseline case x_{VG} = 1.54 m.

in ZPG and APG boundary-layer flat-plate flow; see also appended Paper 1. The ZPG experiments were carried out in the minimum-turbulence-level wind tunnel at KTH, and the APG case for the comparison study was the one given in section 5.1.

Figures 5.3 and 5.4 present the combined near-field and far-field $\overline{u'v'}(y)$ and $\overline{u'u'}(y)$ stress distributions for the ZPG case. Each of the top left distributions represents the initial distributions at the VVG model forcing plane. The original VVG model $\Delta\overline{u'v'}(y)$ stresses without the forcing term were initially zero but, when traveling downstream, primarily produced via the turbulence production $\mathcal{P}_{12}$, as can be seen from the top plots in figure 5.3. The $\overline{u'u'}(y)$ stresses were not provided by the original VVG model, and the variation in the streamwise direction was rather slow, as can be seen in the top plots in figure 5.4.

On the other hand, the results for the improved VVG model showed improved stress distributions for the $\overline{u'v'}(y)$ and the $\overline{u'u'}(y)$ stresses, matching the fully-resolved results well above the vortex center, viz. $y/h_{\mathrm{VG}} > 1$. Below the vortex center, the stress distributions showed a deficit when compared to the fully-gridded results, but they approached each other through turbulence production and redistribution further downstream. The improved model stresses converged reasonably well with fully-gridded results. With the beginning of the far field, the stresses for both VVG models approached and lay on top of each other for $x/h_{\mathrm{VG}} > 9.4$. The process of mutual approach is the result of the diffusive, productive, and redistributive effects within the DRSM. Both VVG models showed lower stress levels in the distant far field when compared to the fully three-dimensional computations and experiments, which resolved the vortex structures which have longer life times than the modelled vortex stresses.

As for the original VVG model in section 5.1, the APG flat-plate boundary-layer computations were carried out for the improved VVG model and compared to computations without VVGs, with the original VVG model, and also to fully-resolved VVG results; see also figure 5.5. The boundary conditions for the boundary layer without flow control and for the improved VVG model were identical to those for the original VVG model from section 5.1. The baseline case for a forcing plane at $x_{\mathrm{VG}} = 1.54$ m was examined and is compared in figure 5.5. The improved VVG model gives a substantial increase of local skin-friction in the near-field transient. The increase of the skin-friction peak is almost identical to the fully-resolved data; cf. VG3D. The improved VVG model eliminated the separation bubble efficiently, and provided a more accurate prediction for separated flow, i.e. $c_f < 0$, as compared to the original VVG model.

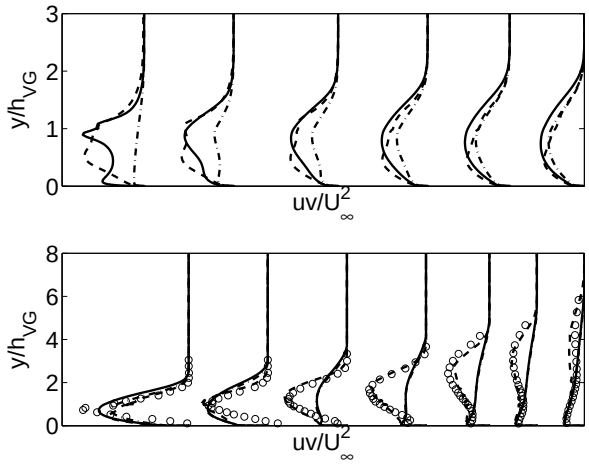

FIGURE 5.3. Original VVG model (broken line), improved VVG model (solid line), spanwise-averaged fully-resolved computational (dashed line), and spanwise-averaged experimental (circles) results for: near field $x/h = 0.0$, 0.5, 1.1, 1.7, 2.2, and 2.8 (top); far field $x/h = 3.3$, 9.4, 23, 37, 65, 93, and 148 (bottom).

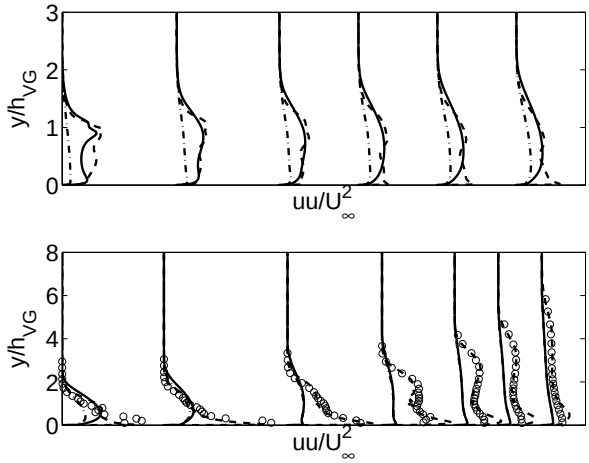

FIGURE 5.4. Original VVG model (broken line), improved VVG model (solid line), spanwise-averaged fully-resolved computational (dashed line), and spanwise-averaged experimental (circles) results: near field $x/h = 0.0$, 0.5, 1.1, 1.7, 2.2, and 2.8 (top); far field $x/h = 3.3$, 9.4, 23, 37, 65, 93, and 148 (bottom).

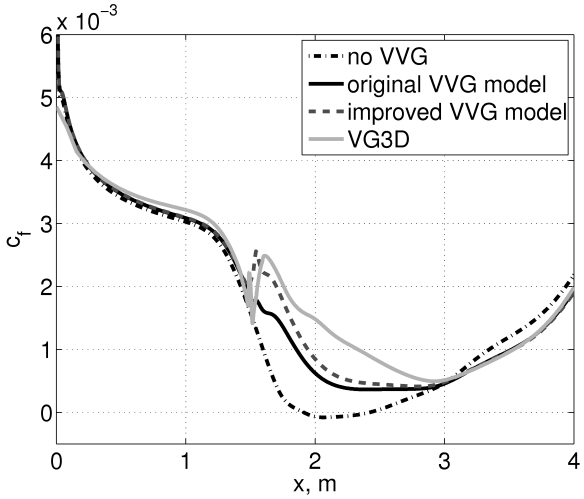

FIGURE 5.5. Local skin-friction coefficient distributions for the baseline case $x_{\mathrm{VG_{TE}}} = 1.54$ m: no VVGs applied, for the original and the improved VVG model computations, and for the spanwise-averaged fully-resolved computations (VG3D).

5.3. VVG Model Applications

5.3.1. *HELIX Airfoil with Short-Chord Flap*

The original VVG model was applied to model a corotating VVG array in the turbulent boundary layer of the HELIX airfoil short-chord flap; see also appended Paper 5. Several VVG settings were computationally investigated within this project and the initial VVG model position ($x_{\mathrm{VG}} = 25\%\ c_{\mathrm{flap}}$) was not capable to suppress separated flow as in corresponding experiments; see figure 5.6(a). The reason for this was found to be the large detached-flow region on the short-chord flap that was deployed at higher angle of attacks α when compared to a conventional high-lift system. In contrast to the VVG model RANS computations, flow-separation control worked well in the experiments as a result of the strongly fluctuating flow around the flap, which enabled the creation of streamwise vortices when attached flow impinged the VVGs. Such flow conditions could not be achieved by a RANS computation which solves for the steady-state ensemble-averages and cannot capture unsteady flow states.

Nevertheless, it could be shown that the VVG model could successfully prevent flow separation on the flap for different configurations. The main parameter was found to be the streamwise location of the VVG on the flap. Figure 5.6(b) shows the flow state for a setup with the VVG located further upstream in the permanent-attached flow region at 8% c_{flap}. It can also be seen that the VVG model establishes attached flow around the entire short-chord flap. Furthermore, the modelled VVG shape and height were changed during in this

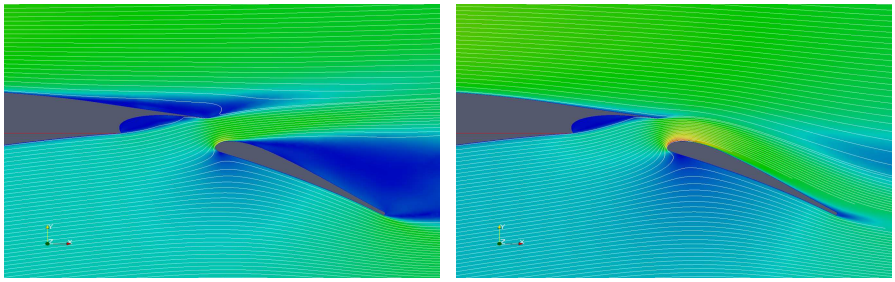

(a) (b)

FIGURE 5.6. Velocity contours (blue: low velocity; red: high velocity), and streamline plots for: (a) the original airfoil without VVG model, and (b) the modified airfoil with the original VVG model applied.

study, and the mean flow showed some sensitivity for the setup parameters. As a result of the study, the VVG position can be said to be the most important VVG model parameter, followed by the VVG height which has a direct influence on the magnitude of $\Gamma_{\max}$ due to its dependency on the VVG tip velocity.

5.3.2. *Plane Asymmetric Diffuser Flow*

A further comparison between the original and the improved VVG models was carried out in the APG section of a plane asymmetric diffuser with an opening angle of 8.5°; see appended Paper 1. The 8.5° opening angle gives a weak separation which can be easily controlled, and this flow case was therefore suitable for an evaluation of the VVG models. Computations without any flow control revealed a separated region on the upper diffuser wall, see figure 5.7(a), which was in good agreement when compared to the experiments by Törnblom (2006). Applying the original VVG model established attached flow, see figure 5.7(b), and the pressure coefficient results showed a clear increase in static pressure on the upper wall (not shown here). When applying the improved VVG model, it could be observed how the streamlines were pushed further upward, and even how a slight separated region was generated on the lower diffuser wall; figure 5.7(c). Pressure coefficient curves showed a prevailing increase in static pressure throughout the diffuser when compared to the results for the original VVG model. As a result, the application of the improved VVG model led to a slightly higher pressure recovery at the diffuser exit, similar to that from the experiments with VVGs. In figure 5.7(c), it can be seen from the increased turbulence kinetic energy contours that the influence of the improved VVG model is stronger in the near field close to the upper wall.

Whether the results from the original or the improved VVG model results are correct could not be conclusively answered, because detailed velocity plots

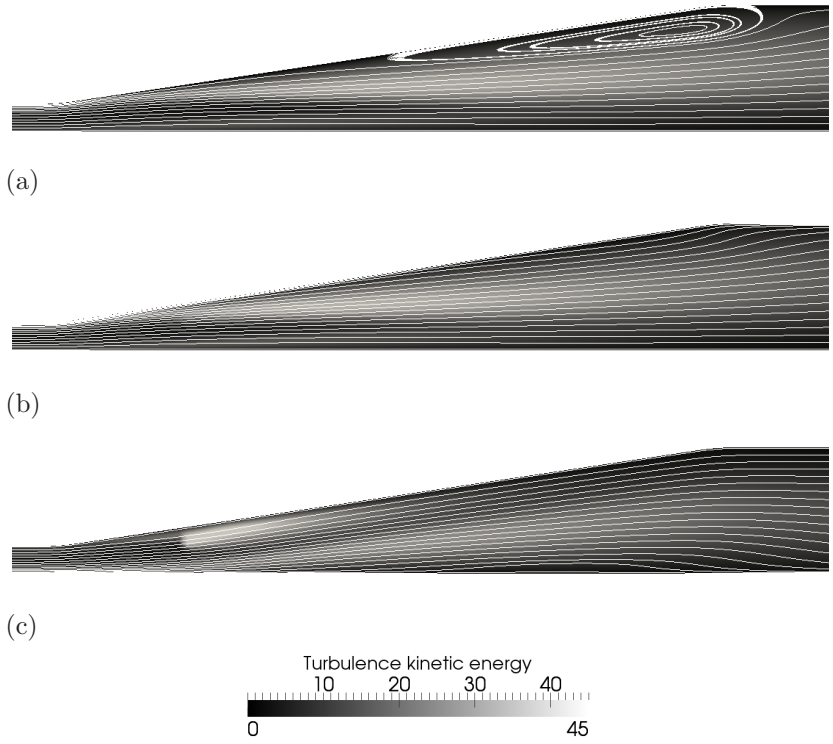

FIGURE 5.7. Turbulence kinetic-energy contours and streamlines for the computations: (a) without VG model, (b) with original VG model, and (c) with improved VG model.

within the diffuser, as well as a pressure-coefficient distributions on the lower wall were not available for experiments with VVGs. In total, it can be stated that the improved VVG model has a stronger impact on the near field characteristics, which led to a higher pressure recovery at the diffuser exit. But, on the other hand, this also gives fundamentally different flow states for the rather sensitive flow case of the plane asymmetric diffuser.

5.4. Parameterization of VGJ Experiments

As the motivation was to develop a statistical model also for active VGJs, a collaboration with the Institute of Fluid Mechanics of Technische Universität Braunschweig, Germany, was initiated by the author; see also appended Paper 3. Experimental results for single VGJs (Ortmanns 2008) and VGJ pairs (Casper 2011), comprising a broad range of parameter variations regarding α, β, U_∞, and λ were examined at KTH. The single-jet data were analysed using the velocity triple decomposition, and experimental vortex velocities $U_i(y, z)$ could be extracted from the analysis. The results could be used to carry out

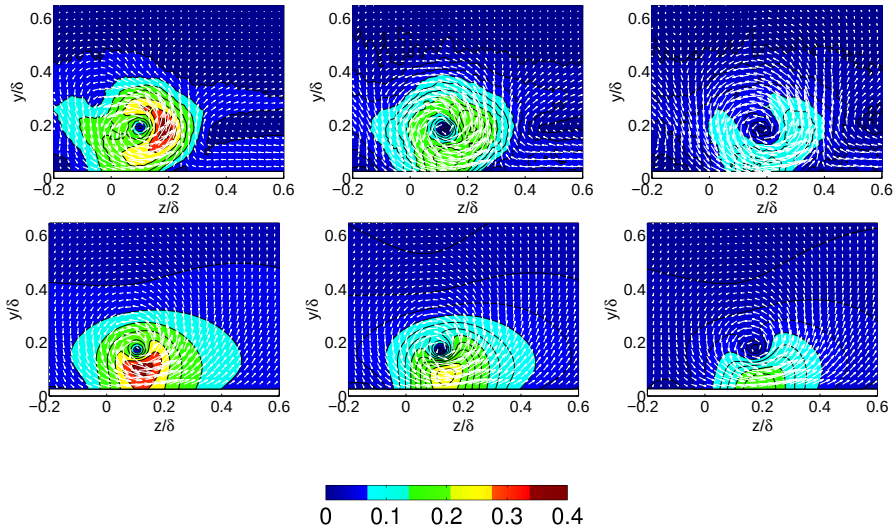

FIGURE 5.8. Experimental (top) and fitted (bottom) vortex-velocity fields $\sqrt{(V_y^2 + V_z^2)}/U_\infty$ at streamwise positions $x =$ 50, 100, and 200 mm (from left to right.). Here: $U_\infty = \mathbf{25}$ $\mathbf{m/s}$, $\lambda = \mathbf{2.5}$, $\alpha = \mathbf{45}^\circ$, $\beta = \mathbf{90}^\circ$.

a nonlinear least-squares data fitting between the experimental single-jet vortex velocities $U_i(y, z)$ and the Lamb-Oseen vortex-model velocity $V_i(y, z)$. The data fitting resulted in fitted parameters for $\Gamma_{\max}$, r_0, and (h_c, z_c).

A comparison of the streamwise development of an experimental vortex and a fitted Lamb-Oseen vortex at three streamwise locations is presented in figure 5.8. A reasonably good agreement between experiments and the fitted vortex is given. Still, differences in the secondary-flow field can be observed because the Lamb-Oseen vortex model represents a simplified description of the experimental vortices. The experiments show secondary-vortex flow as well as peak velocities between the primary and seconday vortices, whereas the modelled vortex velocity develops its peak values between the wall and the vortex core. The fitted results are satisfactory, and figure 5.8 is representative for a broad parameter range of β, U_∞, and λ, for which the least-squares fitting worked well.

The results of the nonlinear least-squares data fitting for $r/r_0 \leq 8$ are presented in figure 4.6 in section 4.5. The general conclusion from this figure is that the modelling of experimental results was successfully accomplished by means of the Lamb-Oseen vortex model. Therefore, the Lamb-Oseen vortex model was used for the development of a statistical VGJ model; see section 5.5 and appended Paper 4.

5.5. Evaluation of the Statistical VGJ Model

5.5.1. *Streamwise Development of VGJ Model Parameters*

As stated in section 5.4, the Lamb-Oseen vortex model was chosen for the development of a statistical VGJ model. Therefore, the vortex-model parameters $\Gamma_{\max}$, r_0, and h_c needed to be determined in terms of the VGJ setup parameters α, β, λ, U_∞, and Φ_{VGJ}. For the determination of the parameters r_0, and h_c, empirical results from the single-jet experiments by Ortmanns (2008) could be used. It was shown, that r_0 and h_c depend on the actuator exit diameter Φ_{VGJ} and the velocity ratio λ. The model coefficients for r_0 and h_c, reading C_r and C_h, and the streamwise development by means of the vortex-parameterization results from section 5.4 are plotted in figure 5.9.

C_r can be observed to increase roughly linearly in the streamwise direction for all VGJ settings. The $\alpha = 45°$ results show a spread in results, but the reasons for this is unclear. However, the results are still close together when compared to the wide range of parameter settings that were used in the VGJ experiments. Nevertheless, an extrapolation to $x/\delta_{99} = 0$ for the $\alpha = 30°$ results is proposed in order to determine inital setting for C_r for the statistical VGJ model. Thereby, a universal value $C_r = 0.4$, valid for all settings, was chosen for the application of the VGJ model in ZPG flat-plate boundary-layer flow; see appended Paper 4.

In case of C_h, the same strategy as for C_r was used in order to determine a universal value for the VGJ model. The results for $\alpha = 30°$ lie very close to each other and describe a linear behaviour which can be utilized for a similar extrapolation as for C_r. The $\alpha = 45°$ also show the spread in results. Here, a universal value $C_h = 0.6$ is suggested, which again represents the results for $\alpha = 30°$ very well.

The model coefficient for $\Gamma_{\max}$, C_Γ, was derived analytically in section 4.5. It was shown that $C_\Gamma \approx 0.2$. A comparison of the streamwise evolution for $\alpha = 30°$ from experiments reveals C_Γ-values that lie close together around 0.2; see figure 5.9. The $\alpha = 45°$ values show the typical spread which could be observed for the other nondimensional parameters. However, the agreement between the $\alpha = 30°$ and the theoretical result for C_Γ confirms the idealized model that describes the balance and the transition of momentum between the jet and the vortex reasonably well. Therefore, it can be assumed that the theoretical derivation for C_Γ represents a suitable ansatz for the statistical VGJ model.

In total, it is suggested that $\alpha = 30°$ represents a good setup choice for VGJ flow-separation control, especially when taking the spread in results for $\alpha = 45°$ into account.

5.5.2. *Application of the VGJ Model in ZPG Boundary-Layer Flow*

Figure 5.10 shows the application of the statistical VGJ model in ZPG flat-plate boundary-layer flow in terms of a comparison of $\Delta\overline{v'v'}$ vortex stress results with

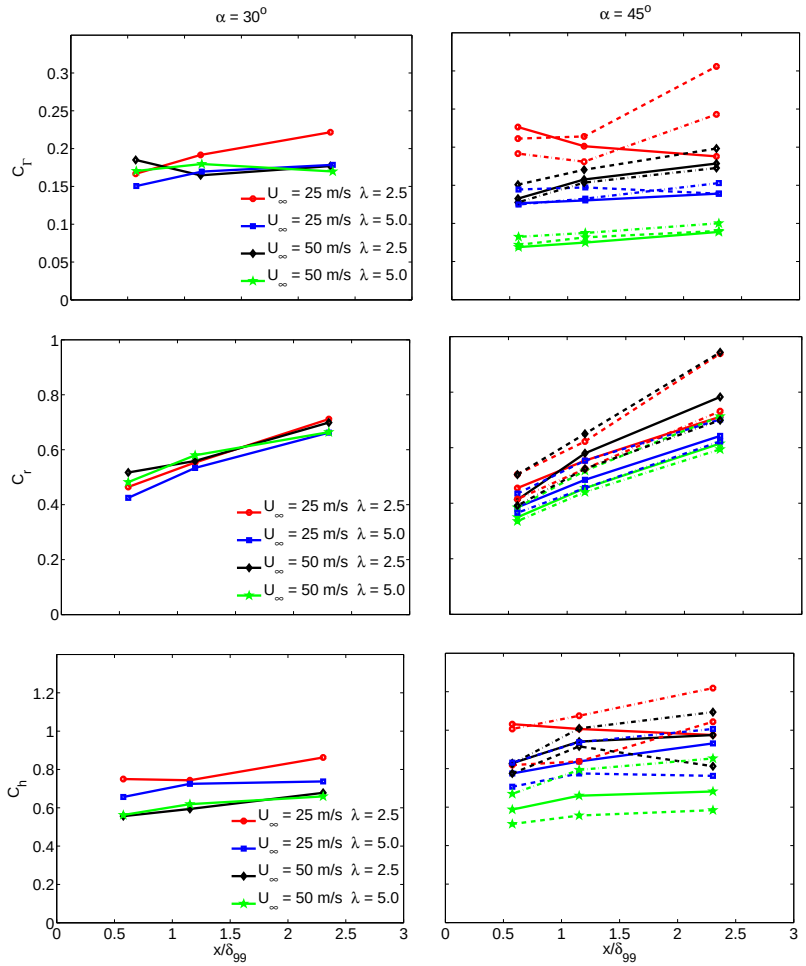

FIGURE 5.9. Streamwise development of the nondimensional VGJ model parameters for experimental results: circulation C_Γ, viscous core radius C_r, and wall-normal location C_h for: $\alpha = \mathbf{30}^\circ$ and $\mathbf{45}^\circ$, $\beta = \mathbf{75}^\circ$ (dashed line), $\mathbf{90}^\circ$ (solid line) and $\mathbf{105}^\circ$ (broken line).

corresponding data from fully-gridded VGJ computations, and experiments. The near-field reveals large vortex-stress differences between the VGJ model and the fully-gridded results, and the reason for this is very likely the vortex formation which takes time/space to develop in the three-dimensional computations. In case of the VGJ model, the vortex stresses already represent fully-developed vortices. Therefore, the vortex stresses do not coincide qualitatively

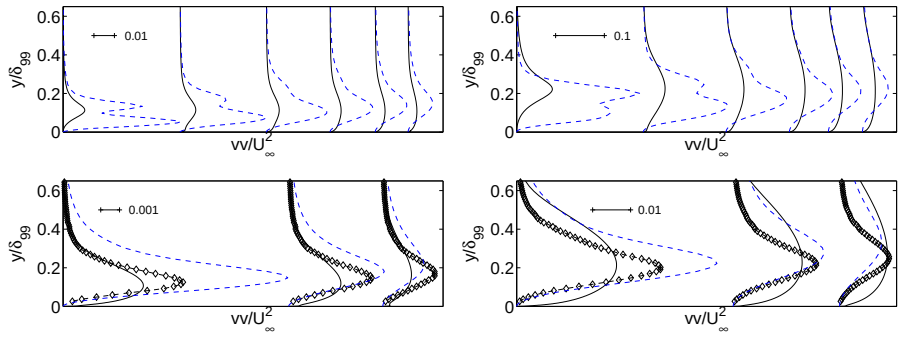

FIGURE 5.10. $\Delta\overline{v'v'}$ vortex-stress distributions. $\alpha = 30°$, $\beta = 90°$, $U_\infty = 25$ m/s, $\lambda = 2.5$ (left), and 5.0 (right): fully-gridded VGJs (dashed line), experiments (circles), and VGJ modelling results (solid line) at $x/\delta_{99} = 0$, 0.1, 0.2, 0.3, 0.4, 0.6 (top), and 0.6, 1.1, and 2.3 (bottom).

in the near field. On the other hand, it can be seen that the far-field stress distributions for the VGJ model represent the fully-resolved computations and the experiments qualitatively well. Still, the VGJ model underpredicts the stresses but the overall streamwise development is very satisfactory for this new VGJ model approach. However, the VGJ model should be tested more thoroughly in APG flows in order to investigate its applicability for more challenging flow conditions.

CHAPTER 6

Summary of Appended Papers

6.1. Paper 1

Vortex-Generator Models for Zero- and Adverse-Pressure-Gradient Flows.

This publication presents the application of the original and the improved VVG model for three different flow cases. First, basic studies, including the calibration and the evaluation of the original and the improved VVG models with experimental data were investigated in ZPG flat-plate boundary-layer flow; see also Lögdberg *et al.* (2009). The setup for the VVG models corresponds to the experimental setup, and a parameter study was carried out using the original VVG model. Based on a basic setup case, the local airfoil-section lift slope K in the LLT, the viscous core radius r_0 in the vortex model, and the turbulent specific dissipation rate ω in the turbulence model were investigated independently of each other. It was shown that changing K had a weak impact on results, whereas the latter two parameters showed stronger dependencies. The improved VVG model constants from equation (4.19) were empirically determined, and it could be shown how the combined stresses improved in the near field downstream of the VVG. In summary, this study showed that the VVG models significantly changed the development and the distribution of stresses, including the near-field development close to the VVG forcing plane

Second, the VVG models were investigated in an APG flat-plate boundary-layer flow, comparable to the experiments by Lögdberg *et al.* (2010). It could be shown how the two VVG models performed under flow conditions including a separated region, comparable to the suction side of an airfoil. In total, the VVG model generally underpredicted skin-friction results compared to fully-resolved computations, even though the improved VVG model showed better results when compared to the original VVG model. Nevertheless, both VVG models successfully predicted attached flow on the flat plate, and this is in agreement with experiments and fully-resolved computational results.

In a last part, the VVG models were investigated in internal diffuser flow. The results showed that the VVG models generally underpredicted the increase of pressure-coefficient distributions in the expanding part in experiments. The VVG models were still capable of predicting the pressure recovery at the diffuser exit quantitatively correct. On the other hands, both VVG models predicted different flow states within the diffuser, but this could not be evaluated by experiments or fully-resolved computations. Nevertheless, the general findings

regarding the differences of flow-control capabilities between both VVG models from the APG flat-plate case could be confirmed by the diffuser flow case.

6.2. Paper 2

Evaluation of a Vortex Generator Model in Adverse Pressure Gradient Boundary Layers.

This paper presents the evaluation of the original VVG model in APG flat-plate boundary-layer flow which was previously experimentally investigated by Lögdberg (2008). Lögdberg carried out studies including three different APG cases, whereas the computational investigations by the author concentrated on the most comprehensively studied case. The experiences and results from Paper 1 concerning the calibration of the VVG model were used and applied. Moreover, sensitivity studies of the VVG position upstream of the separation bubble complemented the previous research results. It could be shown by means of skin-friction as well as static-pressure distribution plots, that the VVG model showed strong sensitivity for the streamwise position, leading to a better separation prevention in terms of increased skin-friction results the further upstream the VVG model was applied within the APG region. If the VVG model was located too closely to the separated region, flow separation could not be prevented. The VVG was also positioned in the preceeding wind-tunnel ZPG region where the opposite flow-control effect was observed, i.e., decreasing skin-friction distributions for further upstream VVG positions.

Second, it could be shown that the original VVG model was capable of establishing the same overall flow states (attached/detached flow) as in experiments, i.e., when a VVG position variation, as well as a VVG height variation was investigated.

In total, this paper has shown that the original VVG model successfully describes the qualitative impact of passive VVGs on flow-separation control by means of the statistical-modelling approach and by using the original VVG model.

6.3. Paper 3

Evaluation and Parameterization of Round Vortex-Generator-Jet Experiments for Flow Control.

The aim of this study was to parameterize single-jet vortices in terms of the Lamb-Oseen vortex model, as well as to identify and to classify efficient VGJ parameter settings for flow-separation control. The contribution covers the evaluation of the VGJ experiments, previously carried out at Technische Universität Braunschweig, Germany. Single VGJs had been investigated over a broad VGJ parameter range, including variations of α, β, U_∞ and λ. The vortex-velocity fields from experiments were parameterized by means of a non-linear least-squares data fitting to the vortex model velocities. Thereby, fitted vortex-model parameters $\Gamma_{\max}$, r_0, and h_c for each single-jet setup were identified and thereby, allowed for the modelling of the vortex velocities from

experiments. It was shown that the Lamb-Oseen vortex model represented the experimental results well. From that, the spanwise-averaged vortex stresses $\Delta\overline{u_i'u_j'}(y)$ of the modelled vortices could be derived and evaluated over a broad VGJ parameter setup range. A comparison of the single-jet vortex stresses to those for VGJ pairs in a counter-rotating common-flow-down configuration with a similar parameter setup was given, and the results showed high comparability between the single VGJs and the VGJ pairs.

In a second step, the fitted Lamb-Oseen vortex-model parameters $\Gamma_{\max}$, r_0, and h_c were nondimensionalised and a results comparison study for $\alpha = 45°$ at the first near-field measurement plane was carried out. It could be shown that the most important VGJ parameters for the nondimensional parameters was the velocity ratio λ and that there occurs a variation for the skew angle β.

This contribution represented the starting point and provided essential information for the development of a statistical VGJ model for flow-separation control which is presented in Paper 4.

6.4. Paper 4

A Statistical Vortex-Generator-Jet Model for Turbulent Flow-Separation Control.

This paper presents the ansatz for a statistical VGJ model and is, to a large extent, based on the findings of Paper 3. The Lamb-Oseen vortex model was chosen for the modelling of the vortex velocities, because it had shown satisfactory results in Paper 3. The statistical ansatz required the Lamb-Oseen vortex-model input parameters $\Gamma_{\max}$, r_0, and h_c, and in terms of the VGJ, a different approach was necessary when compared to the modelling of VVGs. The vortex generation was found to be fundamentally different for VGJs and therefore, an expression for $\Gamma_{\max}$ which did not originate from the LLT, needed to be determined. Empirical results for r_0 and h_c, similar to the findings for VVGs, were also sought after.

The experimental results and the parameterization study from Paper 3 served as a starting point for the derivation of the fitted vortex-model parameters $\Gamma_{\max}$, r_0, and h_c. Based on that, nondimensional vortex-model parameters C_Γ, C_r, and C_h as functions of the VGJ parameters β, Φ_{VGJ}, U_∞, and λ were successfully determined. Universal-valid empirical values for the nondimensional vortex-model parameters C_r and C_h were found based on the experimental results. An analytical expression for the vortex circulation $\Gamma_{\max}$, and a value for C_Γ were determined by inspecting the balance between the momentum of the injected jet and the momentum of the created fully-developed streamwise vortex further downstream in the flow. The analytical results for C_Γ could be confirmed by experimental results for the term C_Γ, and therefore, it is suggested that the expression for the vortex circulation $\Gamma_{\max}$ is reasonable. The determined nondimensional VGJ model parameters $C_\Gamma = 0.2$, $C_r = 0.4$, and $C_h = 0.6$ were used in the application of the VGJ model in ZPG flat-plate flow. The analysis of results, as well as its comparison to the experiments

and fully-resolved computations gave satisfactory streamwise statistical vortex-stress distributions. In the far field, where the vortices are fully-developed, results for the forced stresses compared mostly qualitatively well and a sensitivity of the VGJ model regarding λ and h_c could be observed. Nonetheless, in order to show the VGJ models's flow-separation capabilities, further evaluation studies should to be carried out.

6.5. Paper 5

Application of a Statistical Vortex Generator Model Approach on the Short-Chord Flap of a Three-Element Airfoil.

This conference paper presents the application of the original VVG model on the short-chord flap of the HELIX three-element airfoil. The challenge that is linked to the design of a short-chord is the higher flap deflection angle δ_F which is required in order to achieve the same total lift force as for a conventional flap. Due to higher δ_F, flow separation is more likely to occur on a short-chord flap, and thus, VVGs may be a way to overcome separated flow on the suction side of the flap.

Experiments with the HELIX airfoil have shown that VVGs are able to prevent flow separation when applied at 25% flap chord c_{flap}. An application of the VVG model with a corresponding setup as from the experiments was, on the other hand, not capable of achieving attached flow on the flap. Therefore, different setup-parameter variations for the VVG model were investigated. Results for a streamwise-position variation of the VVG revealed that the DRSM-based VVG model does not work properly when the VVG is located in regions with heavily separated flows. It was found that flow-separation prevention was essentially enabled when the VVG was positioned very close to the flap leading edge. In the same manner, the VVG height has an impact on the flow-separation capabilities since higher vane-tip velocities generate stronger vortex stresses by the VVG model. However, successful flow-separation control could be shown up to 8% c_{flap} which is rather far upstream when compared to experiments (25% c_{flap}). The VVG model showed its capabilities and shortcomings for flow-separation control on an airfoil high-lift system and based on these results, a further development of the original VVG model could be motivated.

CHAPTER 7

Concluding Remarks and Outlook

This thesis deals with flow-separation control by means of VVGs as well as VGJs, and the methods to model these flow-separation-control devices in a statistical sense.

The statistical VVG model has been evaluated by means of different flow cases in this thesis: ZPG and APG flat-plate boundary-layer flow, APG diffuser flow, and the external flow around the HELIX three-element airfoil with a short-chord flap. It could be generally shown that the original VVG model predicts the influence of such passive flow-control devices qualitatively correct. Nevertheless, it could also be observed how the flow-control effect of the original VVG model was in many cases lower than expected, for example when compared to corresponding experiments or fully-resolved VVG computational results. As discussed in section 5.2, the $\overline{u'v'}$ Reynolds stresses are generated through the production term $\mathcal{P}_{12}$ in the turbulence model that, in turn, need a certain streamwise distance to properly develop. This causes a large variation of the $\overline{u'v'}$ Reynolds stresses in the near field, as can be seen in figure 5.3. Nonetheless, the original VVG model showes very satisfactory results in an APG flat-plate boundary-layer and diffuser flow, preventing flow separation as predicted by fully-resolved computations and experiments.

An improved statistical VVG model was developed based on the original VVG model which enables a direct forcing of the additional vortex stresses $\Delta\overline{u'u'}$ and $\Delta\overline{u'v'}$. Thus, the important shear stresses $\Delta\overline{u'v'}$ can directly act from the improved VVG model forcing plane, and are able to to mix the boundary layer even in the very near field. The development of the improved VVG model represents a more comprehensive flow-separation-control model and its potential should be examined further in the future. The HELIX airfoil case represents an adequate flow case for that, because original VVG results are available; see section 5.3. The improved VVG model may be able to describe the prevention of flow separation also for VVG closer to 25% c_{flap}, so that results may become more comparable to experiments.

In terms of flow-separation control with VGJs, experimental and computational data were analysed in this thesis. It was assumed that VGJ arrays may be represented by single VGJs when the design criteria of a certain minimum VGJ actuator distance D is fulfilled. A parameterization of the experimental single-jet results by means of a nonlinear least-squares data fitting led to a validation of the Lamb-Oseen vortex model to sucessfully represent fully-developed

vortices from single VGJs. Dependencies of the Lamb-Oseen vortex-model parameters on the VGJ parameters have shown that the vortex circulation $\Gamma_{\max}$ was dependent on the freestream Reynolds number, the velocity ratio λ, and, for high U_{VGJ}, also on the Mach number Ma. A higher value for λ increased the vortex strength and efficiency of the jet, whereas compressible effects for high λ showed opposite trends when compared to low Ma cases.

In another study, the statistical VGJ model was evaluated in ZPG flat-plate boundary-layer flow. The results showed reasonably good agreement with fully-resolved RANS computations, as well as with experiments. Parameter variations for λ and U_{VGJ} were carried out and vortex stress results downstream of the VGJ were presented. The VGJ model results are considered to be satisfactory for the first ansatz of this idealized statistical VGJ model.

For future studies, it is suggested to apply the VGJ model to APG boundary-layer flows, similar to those of the investigations for the VVG models. A direct comparison between VGJ model and corresponding fully-resolved VGJ computations may illustrate interesting differences concerning the flow-separation control capabilities of VGJs. An improved description of the VGJ model, similar to the improved VVG model, should be considered as a next logical step towards an enhanced VGJ model. Even though the vortex creation for active VGJs is fundamentally different compared to the distinct vortex-shedding from passive VVGs, such an improvement could ameliorate the flow-separation-control abilities of the VGJ model in the very near field behind the VGJ forcing plane.

In terms of the investigated flow cases for the VGJ model, LES analyses have the potential to also resolve for the small-scale turbulent eddies, as well as the momentum mixing in the shear layer between the incoming turbulent boundary layer and the jet. They may play, although the opposite was reported by some researchers, an important role in the final vortex creation, development and its decay. An option to extend the current VGJ model for periodic excitation would also be a consideration, which has shown to be more efficient than steady-jet blowing. One option could be to establish the time-dependent application of vortex stresses in the flow or, as a second and more realistic alternative, to find an expression for the given "steady blowing" statistical VGJ model in terms of nondimensional parameters C_Γ, C_r, and C_h that may represent an equivalent to the periodic excitation mode.

CHAPTER 8

Papers and Authors' Contributions

Paper 1

Vortex-Generator Models for Zero- and Adverse-Pressure-Gradient Flows
F. von Stillfried (FS), S. Wallin (SW) & A.V. Johansson (AJ), 2012, AIAA Journal **50**(4), pp. 855 – 866,
DOI: 10.2514/1.J051169.

This work is of computational character on the development and the evaluation of two statistical VVG models for passive VVGs in ZPG and APG flat-plate boundary-layer flow. The computations, the data analysis, as well as the writing was done by FS with considerable help and supervision by SW and AJ. SW provided results for the diffuser study. Parts of these results have been presented and published in:

Statistical Modeling of the Influence of Turbulent Flow Separation Control Devices
F. von Stillfried, S. Wallin & A.V. Johansson, 2009, 47^{th} AIAA Aerospace Sciences Meeting, Orlando, FL, USA, AIAA Paper 2009-1501.

Statistical Modeling of Vortex Generators in Pressure Gradient Boundary Layers
F. von Stillfried, S. Wallin & A.V. Johansson, 2009, Sixth International Symposium on Turbulence and Shear Flow Phenomena, Seoul National University, Seoul, Korea, Conference Proceedings, Vol. II, pp. 647-652.

An Improved Passive Vortex Generator Model for Flow Separation Control
F. von Stillfried, S. Wallin & A.V. Johansson, 2010, 5^{th} AIAA Flow Control Conference, Chicago, IL, USA, AIAA Paper 2010-5091.

Paper 2

Evaluation of a Vortex Generator Model in Adverse Pressure Gradient Boundary Layers

F. von Stillfried (FS), S. Wallin (SW) & A.V. Johansson (AJ), 2011, AIAA Journal **49**(5), pp. 982 – 993,
DOI: 10.2514/1.J050680.

This work is of computational character on the evaluation of the original statistical VVG model in APG flat-plate boundary-layer flow. The computations, the data analysis, as well as the writing was done by FS with considerable help and supervision by SW and AJ. Parts of these results have been presented and published in:

Statistical Modeling of Vortex Generators in Pressure Gradient Boundary Layers

F. von Stillfried, S. Wallin & A.V. Johansson, 2009, Sixth International Symposium on Turbulence and Shear Flow Phenomena, Seoul National University, Seoul, Korea, Conference Proceedings, Vol. II, pp. 647-652.

Paper 3

Evaluating and Parameterizing Round Vortex Generator Jet Experiments for Flow Control

F. von Stillfried (FS), S. Wallin (SW), A.V. Johansson (AJ), M. Casper (MC) & J. Ortmanns (JO), 2012,
accepted for publication in AIAA Journal.

This work is of experimental and analytical character and deals with the evaluation of VGJs in a ZPG flat-plate boundary-layer flow. The experiments were carried out by JO and MC at Technische Universität Braunschweig, Germany. The data analysis and the writing was done by FS with considerable help and supervision by SW and AJ, as well as with inputs from JO and MC. Parts of these results have been presented and published in:

Evaluating Vortex Generator Jet Experiments for Turbulent Flow Separation Control

F. von Stillfried, T. Kékesi, S. Wallin & A.V. Johansson, 2011, European Turbulence Conference 13, Warsaw, Poland, *Journal of Physics: Conference Series 318 022038*, DOI:10.1088/1742-6596/318/2/022038.

Paper 4

A Statistical Vortex-Generator-Jet Model for Turbulent Flow-Separation Control

F. von Stillfried (FS), S. Wallin (SW) & A.V. Johansson (AJ), 2012, submitted to AIAA Journal.

This work is of computational character on the development of a statistical VGJ model for active VGJs. The data analysis and the writing was done by FS with considerable help and supervision by SW and AJ. Parts of these results have been presented and published in:

A Novel Modeling Approach for Vortex Generator Jet Flow Separation Control
F. von Stillfried, S. Wallin & A.V. Johansson, 2012, 50^{th} AIAA Aerospace Sciences Meeting, Nashville, TN, USA, AIAA Paper 2012-0742.

Paper 5

Application of a Statistical Vortex Generator Model Approach on the Short-Chord Flap of a Three-Element Airfoil

F. von Stillfried (FS), S. Wallin (SW) & A.V. Johansson (AJ), 2009, presented at the KATnet II conference on Key Aerodynamic Technologies, 12-14 May, Bremen, Germany

This work is of computational character on the development of the original VVG model in APG boundary-layer flow of a three-element airfoil. The basic computational grid as well as the experimental data were provided by Ulf Tengzelius of FOI. The data analysis and the writing was done by FS with considerable help and supervision by SW and AJ.

Acknowledgements

No book is ever the product of only one individual's efforts, and it is clear that this one is not any different. I could never have realised it without the help and suggestions of many supportive friends and colleagues.

I would like to express my sincere thanks to my supervisors, Arne Johansson and Stefan Wallin, for their guidance and the very fruitful and enlightning meetings, as well as for their support during all the time. Moreover, I am very thankful for the numerous and accurate discussions with Arne and Stefan that significantly increased the quality of the submitted papers.

I am grateful for the support and the helpful comments of Ola Lögdberg of Scania AB, Sweden, concerning his experimental work on VVGs at KTH which were essential for the comparison studies that I carried out.

Moreover, I am glad to have experienced a very welcoming and friendly working atmosphere during my entire stay at the Institute of Fluid Mechanics of Technische Universität Braunschweig, Germany, and I especially thank Marcus Casper and Peter Scholz for the successful cooperation, the support, and the kind provision of experimental data within our collaborative research project on VGJs. Jens Ortmanns of Rolls-Royce Germany is highly acknowledged for the very kind and straightforward assistance concerning his former PhD project on VGJs.

During my time as a PhD candidate, I have been quite many times at FOI in Kista, and I have to mention at least the following colleagues for their support from which I benefitted during the last years: Peter Eliasson and Olof Grundestam for their comprehensive support concerning the CFD code Edge, Ulf Tengzelius who helped me with the HELIX airfoil case, Henrik Edefur for his assistance in mesh-generation techniques in ICEM, and Oskar Enoksson for the support regarding the tunnan computer cluster.

Many special thanks to my former and present office colleagues, as well as to everybody from the department who regularly played indoor hockey with me; good times I will never forget. Moreover, I have always experienced a very friendly working atmosphere at KTH Mechanics and I feel very much indebted to all the above individuals, and to those colleagues who have crossed my ways whose names I have not listed, and who have assisted, inspired, and enlightened me one way or another ever since I started working at KTH in September 2007.

Furthermore, the financial support of the Erich-Becker foundation of Fraport AG, Germany, is highly appreciated.

Last but not least I take full responsibilty for misapprehensions, omissions and oversimplifications in this thesis. Nonetheless, I hope that the rest of this book creates new insights and gives new knowledge to the flow-control community.

Thank you all.

Stockholm, May 2012
Florian von Stillfried

References

Barth, T., Scholz, P. & Wierach, P. 2011 Flow Control by Dynamic Vane Vortex Generators Based on Piezoceramic Actuators. *AIAA Journal* **49** (5), 921 – 931.

Bender, E. E., Anderson, B. H. & Yagle, P. J. 1999 Vortex Generator Modelling for Navier-Stokes Codes. *American Society of Mechanical Engineers, FEDSM 99-6919*.

Casper, M. 2011 Personal communication.

Compton, D. A. & Johnston, J. P. 1992 Streamwise Vortex Production by Pitched and Skewed Jets in a Turbulent Boundary Layer. *AIAA Journal* **30** (3), 640 – 647.

Dudek, J. C. 2006 Empirical Model for Vane-Type Vortex Generators in a Navier-Stokes Code. *AIAA Journal* **44** (8), 1779 – 1789.

Dudek, J. C. 2011 Modeling Vortex Generators in a Navier-Stokes Code. *AIAA Journal* **49** (4), 748 – 759.

Glauert, H. 1926 *The Elements of Aerofoil and Airscrew Theory*, 1st edn. Cambridge University Press, London, UK.

Gleyzes, C. & Pailhas, G. 2011 Flow Control using Continuous Fluidic Vortex Generators. Validation of a Simple CFD Model of the Interaction Between a Boundary Layer and an Inclined Jet. *AIAA Paper 2011-3849*.

Godard, G. & Stanislas, M. 2006 Control of a Decelerating Boundary Layer. Part 1: Optimization of Passive Vortex Generators. *Aerospace Science and Technology* **10** (3), 181 – 191.

Jirásek, A. 2005 A Vortex Generator Model and its Application to Flow Control. *Journal of Aircraft* **42** (6), 1486 – 1491.

Johnston, J. P., Mosier, B. P. & Khan, Z. U. 2002 Vortex Generating Jets: Effects of Jet-Hole Inlet Geometry. *International Journal of Heat and Fluid Flow* **23**, 744 – 749.

Johnston, J. P. & Nishi, M. 1990 Vortex Generator Jets – Means for Flow Separation Control. *AIAA Journal* **28** (6), 989 – 994.

Khan, Z. U. & Johnston, J. P. 2000 On Vortex Generating Jets. *International Journal of Heat and Fluid Flow* **21**, 506 – 511.

Lin, J. C. 2002 Review of Research on Low-Profile Vortex Generators to Control Boundary-Layer Separation. *Progress in Aerospace Sciences* **38**, 389 – 420.

Lin, J. C., Selby, G. & Howard, F. 1991 Explority Study of Vortex-Generating Devices for Turbulent Flow Separation Control. *AIAA 1991-0042*.

Lögdberg, O. 2008 Turbulent Boundary Layer Separation and Control. PhD thesis, Department of Mechanics, KTH Stockholm.

Lögdberg, O., Angele, K. & Alfredsson, P. H. 2010 On the Robustness of Separation Control by Streamwise Vortices. *European Journal of Mechanics B/Fluids* **29** (1), 9 – 17.

Lögdberg, O., Fransson, J. H. M. & Alfredsson, P. H. 2009 Streamwise Evolution of Longitudinal Vortices in a Turbulent Boundary Layer. *Journal of Fluid Mechanics* **623**, 27 – 58.

Mahmood, S. & Radespiel, R. 2009 RANS Simulation of Jet Actuation in a Boundary Layer-Flow using Chimera Grids. *Deutscher Luft- und Raumfahrtkongress, September 8-10, Aachen, Germany*.

Mahmood, S. & Radespiel, R. 2011 Detached-Eddy Simulation of Vortex Generator Jet using Chimera Grids. *International Conference on Computational Fluid Dynamics, July 27-29, Paris, France*.

Ortmanns, J. 2008 Aktive Grenzschichtbeeinflussung mittels Pneumatischer Wirbelgeneratoren bei großen Reynoldszahlen. PhD thesis, Institut für Strömungsmechanik, Technische Universität Braunschweig.

Ortmanns, J. & Kähler, C. J. 2007 The Effect of a Single Vortex Generator Jet on the Characteristics of a Turbulent Boundary Layer. *International Journal of Heat and Fluid Flow* **28**, 1302 – 1311.

Pauley, W. R. & Eaton, J. K. 1988 Experimental Study of the Development of Longitudinal Vortex Pairs Embedded in a Turbulent Boundary Layer. *AIAA Journal* **26** (7), 816 – 823.

Pearcey, H. H. 1961 Part IV: Shock-Induced Separation and its Prevention by Design and Boundary Layer Control. In *Boundary Layer and Flow Control, its Principles and Applications* (ed. G. V. Lachmann), pp. 1170 – 1344. Pergamon, Oxford, UK.

Pope, S. B. 2000 *Turbulent Flows*. Cambridge, UK: Cambridge University Press.

Prandtl, L. 1921 Applications of Modern Hydrodynamics to Aeronautics. *Tech. Rep* Rept. No. 116. NACA.

Selby, G. V., Lin, J. C. & Howard, F. G. 1992 Control of Low-Speed Turbulent Separated Flow using Jet Vortex-Generators. *Experiments in Fluids* **12**, 394 – 400.

von Stillfried, F., Wallin, S. & Johansson, A. V. 2011*a* Evaluation of a Vortex Generator Model in Adverse Pressure Gradient Boundary Layers. *AIAA Journal* **49** (5), 982 – 993.

von Stillfried, F., Wallin, S. & Johansson, A. V. 2011*b* Vortex-Generator Models for Zero- and Adverse-Pressure-Gradient Flow. *AIAA Journal* **50** (4), 855 – 866.

Törnblom, O. 2006 Experimental and Computational Studies of Turbulent Separating Internal Flows. PhD thesis, Department of Mechanics, KTH Stockholm.

Törnblom, O. & Johansson, A. V. 2007 A Reynolds Stress Closure Description of Separation Control with Vortex Generators in a Plane Asymmetric Diffuser. *Physics of Fluids* **19** (115108).

Wendt, B. J. 2004 Parametric Study of Vortices Shed from Airfoil Vortex Generators. *AIAA journal* **42** (11), 2185 – 2195.

Wilcox, D. C. 1988 Reassessment of the Scale Determining Equation for Advanced Turbulence Models. *AIAA Journal* **26** (11), 1299 – 1310.

Yao, C.-S., Lin, J. C. & Allan, B. G. 2002 Flow-Field Measurement of Device-Induced Embedded Streamwise Vortex on a Flat Plate. *AIAA Paper 2002-3162*.

Zhang, X. 2003 The Evolution of Co-Rotating Vortices in a Canonical Boundary-Layer with Inclined Jets. *Physics of Fluids* **15** (12), 3693 – 3702.

Zhang, X. & Collins, M. W. 1997 Nearfield Evolution of a Longitudinal Vortex Generated by an Inclined Jet in a Turbulent Boundary Layer. *Journal of Fluids Engineering* **119**, 934 – 939.